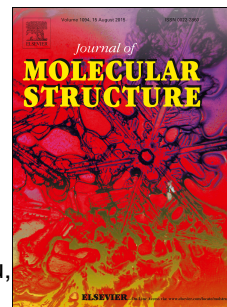


Accepted Manuscript

Mesomorphic properties of Chiral Three-arm Liquid Crystals Containing 1,2,4-Butanetriol as Core

Mei Tian, Shuang-jie Wu, Xiao-Wei Tian, Dan-Shu Yao, Chong-Liang Li, Jian-She Hu, Bao-Yan Zhang



PII: S0022-2860(15)30444-0

DOI: [10.1016/j.molstruc.2015.11.040](https://doi.org/10.1016/j.molstruc.2015.11.040)

Reference: MOLSTR 21990

To appear in: *Journal of Molecular Structure*

Received Date: 17 July 2015

Revised Date: 12 November 2015

Accepted Date: 18 November 2015

Please cite this article as: M. Tian, S.-j. Wu, X.-W. Tian, D.-S. Yao, C.-L. Li, J.-S. Hu, B.-Y. Zhang, Mesomorphic properties of Chiral Three-arm Liquid Crystals Containing 1,2,4- Butanetriol as Core, *Journal of Molecular Structure* (2015), doi: 10.1016/j.molstruc.2015.11.040.

This is a PDF file of an unedited manuscript that has been accepted for publication. As a service to our customers we are providing this early version of the manuscript. The manuscript will undergo copyediting, typesetting, and review of the resulting proof before it is published in its final form. Please note that during the production process errors may be discovered which could affect the content, and all legal disclaimers that apply to the journal pertain.

Mesomorphic properties of Chiral Three-arm Liquid Crystals Containing 1,2,4- Butanetriol as Core

Mei Tian¹, Shuang-jie Wu¹, Xiao - Wei Tian², Dan - Shu Yao¹, Chong - Liang Li¹, Jian - She Hu¹, Bao - Yan Zhang¹

¹Centre for Molecular Science and Engineering, Northeastern University, Shen-yang 110004, People's Republic of China.

² Heilongjiang University, Harbin, 150080, People's Republic of China.

Abstract:

A series of symmetric and asymmetric three-arm liquid crystals (**TALCs**) of which the molecular structure with a central core of 1, 2, 4 - butanetriol attached by three rod-like mesogenic moieties have successfully been synthesized. The rod-like mesogenic side arms are 4' - (4 - (trifluoromethyl) benzoyloxy) biphenyl- 4 - carboxylic acid (TFBA) and 4' - (4 - (allyloxy) benzoyloxy) biphenyl - 4 - carboxylic acid (AOBA), respectively. BTA0 and BTA3 are symmetric **TALCs** with three TFBA or three AOBA as LC side arms, respectively. BTA1 is an asymmetric **TALC** with one AOBA and two TFBA as side arms. BTA2 is an asymmetric **TALC** with two AOBA and one TFBA as side arms. The chemical structures and LC properties of the LC side arms and **TALCs** were characterised by FTIR, ¹H NMR, elemental analysis, DSC, TG, POM and X-ray diffractometer. TFBA displayed smectic B (S_mB) phase, AOBA exhibited nematic (N) phase. The **TALCs** all displayed chiral mesophase properties. BTA0 displayed chiral smectic C (S_mC^*) mesophase. BTA1, BTA2 and BTA3 exhibited cholesteric (*ch*) mesophase. In addition, a chiral smectic A

(S_mA^*) mesophase was observed for BTA1. The results indicated that the 1, 2, 4 - butanetriol is vital in inducing chiral mesophase of the **TALCs**. The side arms also played an important role in the mesophase type and mesogenic region. The **TALCs** displayed cholesteric mesophase when nematic LC side arm AOBA was introduced into the chiral core. The mesogenic region of the **TALCs** increased with the content of the wide-mesophase-region LC side arm AOBA introduced into the **TALCs** increasing. The melting temperature and the clear temperature of the **TALCs** were lower than those of the LC side arms (TFBA and AOBA). The mesophase regions of the **TALCs** were wider than those of the LC side arms.

Key words: chiral star-shaped liquid crystal, symmetric star-shaped, asymmetric star-shaped, three-arm, cholesteric, nematic, smectic

1. Introduction

Cholesteric liquid crystal (LC) materials have attracted considerable interest because of their unique optical and electrical properties, which include selective reflection of light, thermochromism and potential applications such as optical-electro materials [1-8]. As one kind of unconventional LCs, star-shaped LC usually has a core and symmetric or asymmetric mesogens as the side arms. Currently, star-shaped LC has aroused a great deal of interest among chemists because of its symmetric molecular structure and interesting optical properties [9-18]. The common mesophase of star-shaped liquid crystals is columnar [10,13, 19-21]. To the best of our knowledge, cholesteric star-shaped LCs have been described rarely in the past. Yao [15], Zhang

[17] and Saezz [22] have introduced cholesteric mesomorphic arms into a core and obtained cholesteric star-shaped LCs. In these cases, the cholesteric mesomorphic phase of the star-shaped LC was mainly the result of cholesteric mesomorphic arms. We have tried other strategies to obtain cholesteric star-shaped LCs that nematic mesomorphic arms were introduced into chiral cores [23-25]. Glucose, maltose, melitose and sorbitol were adopted as chiral cores. These studies indicate that chiral core is prone to induce the cholesteric phase in the star-shaped LCs with nematic side arms. In these studies, star-shaped LCs are symmetric structure.

Recently Hird [26] summarized the properties and applications of fluorinated liquid crystals. The small size of the fluoro substituent enables its incorporation into all types of liquid crystal, including calamitic, discotic, banana, lyotropic and polymers, without destroying the liquid crystalline nature of the material. However, the fluoro substituent is larger than the hydrogen atom, and hence causes a significant steric effect, which combines with the high polarity, to confer many fascinating and often remarkable modifications to melting point, mesophase morphology and transition temperatures, as well as many other very important physical properties such as dielectric anisotropy, optical anisotropy and visco-elastic properties.

The introduction of trifluoromethyl terminal substituents to calamitic LC is prone to lead to smectic mesophase due to the stronger lateral force of the molecules [27-32], while star-shaped LCs containing trifluoromethyl terminal substituents have been seldom reported. The simultaneous introduction of nematic LC side-arm and smectic LC side-arm containing trifluoromethyl terminal substituents to a chiral core leads to

new chiral asymmetric functional materials. It is necessary to know the effect of the chiral core and both LC side arms on behaviors of star-shaped LCs. In this article, we synthesized a series of symmetric or asymmetric three-arm LCs bearing nematic side arms or smectic side arms containing trifluoromethyl substituents or both the LC side arms based on 1,2,4 - butanetriol.

2. Experimental procedures

2.1. Materials and methods

4 - (Trifluoromethyl) benzoic acid , 4'-hydroxy - 4 - biphenylcarboxylic acid are obtained from Sigma-aldrich without any further purification. 1,2,4 - Butanetriol (*BT*), is obtained from Chengdu Best-reagent Co. *BT* used in this manuscript is a mixture of *S* and *R* isomer, and its specific rotation (in THF) is -2.9° . Ltd. Allyl bromide is obtained from Yancheng Longgang chemical plant. *N,N'* - dicyclohexyl carbodiimide (DCC) and 4 - dimethylamino pyridine (DMAP) are obtained from Shanghai Chemical Industry Company. Hydroxybenzoic acid is obtained from Beijing Reagent Factory. Tetrahydrofuran (THF) is dried over sodium metal and distilled. Pyridine is purified by distillation over KOH before using. Other analytical reagents are used as received.

2.2. Measurement

^1H NMR, ^{13}C NMR and FTIR are measured by Varian WH - 90PFT NMR Spectrometer (Varian Associates, Palo Alto, CA) and Perkinelmer instruments Spectrum One Spectrometer (Perkinelmer, Foster City, CA), respectively. Thermogravimetric analysis (TGA) and DSC measurements are carried out with a

NETZSCH TGA 209C thermogravimetric analyzer, and a NETZSCH instruments DSC 204 (Netzsch, Wittelbacherstrasse, Germany) at a scanning rate of $10^{\circ}\text{C min}^{-1}$ under a flow of dry nitrogen. XRD measurements is performed with nickel-filtered $\text{Cu K}\alpha$ ($\lambda=1.54 \text{ \AA}$) radiation with a D8 ADVANCE XRD (Bruker, Karlsruhe, Germany). The X-ray measurements include wide-angle X-ray diffraction (WAXD) experiments and small-angle X-ray scattering (SAXS) measurements. Measurement of optical rotation (α) is carried out with a PerkinElmer instrument Model 341 Polarimeter at room temperatures using sodium light source ($\lambda=589\text{nm}$). The polarized optical microscopy (POM) study is performed using a Leica DMRX (Leica, Wetzlar, Germany) equipped with a Linkam THMSE - 600 (Linkam, Surrey, England) heating stage.

2.3 Synthesis

The synthetic routes to the mesogenic side arms, 4'- (4 - (trifluoromethyl) benzoyloxy) biphenyl - 4 - carboxylic acid (TFBA) and 4' - (4 - (allyloxy) benzoyloxy) biphenyl - 4 - carboxylic acid (AOBA) are shown in scheme 1.

2.3.1. 4'- (4 - (trifluoromethyl) benzoyloxy) biphenyl - 4 - carboxylic acid (TFBA)

A solution of 4 - (trifluoromethyl) benzoic acid (40g, 0.210mol) and thionyl chloride (40mL) was placed in a round flask equipped with a absorption apparatus to absorb hydrogen chloride. The mixture was stirred at room temperature for 3 h, and heated to 60°C for 10 h to allow the reaction to proceed to completion. The excess thionyl chloride was distilled under reduced pressure. 4 - (trifluoromethyl)benzoyl chloride (TFB - C) was obtained by distillation under reduced pressure (b.p. $105^{\circ}\text{C}/38\text{mmHg}$).

Yield: 87%.

A sample of 4' - hydroxy - 4 - biphenylcarboxylic acid (38.5g, 0.18mol) was dissolved in 80mL dry THF and 20mL dry pyridine. The *TFB - C* (37.4g, 0.18mol) was dissolved in 20mL dry THF. The THF solution of *TFB - C* was added dropwise into the solution of 4' - hydroxy - 4 - biphenylcarboxylic acid. The reaction mixture was refluxed until the result of FTIR analysis showed that the characteristic absorption bands of chloride and hydroxyl disappeared completely and then the solvent was partially removed under reduced pressure. After cooling to room temperature, the residue was poured into 600mL ice water and neutralized with dilute hydrochloric acid. The crude product was obtained by filtration and washed with cold ethanol. The white powder 4' - (4 - (trifluoromethyl) benzoyloxy) biphenyl - 4 - carboxylic acid (TFBA) was obtained after several re-crystallization from ethanol. Yield: 86%. m.p.: 253.5°C. IR (KBr, cm⁻¹): 3063-2560 (-OH in Carboxylic acid dimer), 1739, 1674 (C = O), 1610, 1515 (Ar). ¹H NMR (CDCl₃, d, ppm): 7.186 (s, 2H, Ar - H); 7.553-7.562 (d, *J*=5.4 Hz, 2H, Ar - H); 7.784-7.837 (m, 4H, Ar - H); 8.351-8.526 (m, 2H, Ar - H); 8.708 (s, 2H, Ar - H);

2.3.2. 4' - (4 - (allyloxy) benzoyloxy) biphenyl - 4 - carboxylic acid (AOBA)

4 - (allyloxy)benzoyl chloride (ABA - C) was prepared by 4 - (allyloxy) benzoic acid (ABA was prepared according to ref. 33) and thionyl chloride. A solution of ABA (20 g, 0.11mol) and thionyl chloride (35mL) was placed into a round flask equipped with a absorption apparatus to absorb hydrogen chloride. The mixture was stirred at room temperature for 4 h, and heated to 60°C for 3 h. The excess thionyl chloride was

distilled off under reduced pressure. ABA - C was obtained by distillation under reduced pressure. Yield: 82%.

A sample of ABA - C (27.5g, 0.14mol) was dissolved in 100mL dry THF in a 500mL round flask. 4' - Hydroxy - 4 - biphenylcarboxylic acid (30.0g, 0.14mol) was dissolved in 100mL dry THF and 20mL dry pyridine. The THF solution of ABA-C was added dropwise into the solution of 4' - hydroxy - 4 - biphenylcarboxylic acid. The reaction mixture was refluxed until the result of FTIR analysis showed that the characteristic absorption bands of chloride and hydroxyl disappeared completely and then the solvent was partially removed under reduced pressure. After cooling to room temperature, the mixture was poured into 800mL ice water and neutralized with dilute hydrochloric acid. The crude product was obtained by filtration and washed with cold ethanol. The light yellow powder 4'- (4 - (allyloxy) benzoyloxy) biphenyl - 4 - carboxylic acid (AOBA) was obtained after several re-crystallization from ethanol. Yield: 58%. m.p.: 198.7°C. IR (KBr, cm^{-1}): 3070-2544 (-OH in Carboxylic acid dimer), 2997-2866 (-CH₂), 1729, 1686 (C = O), 1605, 1496 (Ar). ¹H NMR (CDCl₃, d, ppm): 4.405-4.472 (m, 2H, CH₂ = CHCH₂O); 5.349-5.366 (d, *J* = 10.2 Hz, 1H, CH₂ = CHCH₂O); 5.449 - 5.480 (d, *J* = 18.6 Hz, 1H, CH₂ = CHCH₂O); 6.055-6.125 (m, 1H, CH₂ = CHCH₂O); 7.018-7.032 (d, *J* = 8.4 Hz, 2H, Ar - H); 7.270-7.330 (m, 2H, Ar - H); 7.675-7.687 (d, *J* = 7.2 Hz, 4H, Ar - H); 8.111-8.144 (d, *J* = 6.6 Hz, 2H, Ar - H); 8.175-8.215 (d, *J* = 8.0 Hz, 2H, Ar - H);

2.3.2. Tree arms liquid crystals (BTA0-BTA3)

The synthetic routes to butane - 1,2,4 - triyl tris (4' - (4 - (trifluoromethyl) benzoyloxy)

biphenyl-4-carboxylate) (BTA0), 2-(4'-(4-allyloxy)benzoyloxy) biphenylcarbonyloxy) butane-1,4-diyl bis(4'-(4-(trifluoromethyl)benzoyloxy) biphenyl-4-carboxylate) (BTA1), 2-(4'-(4-(trifluoromethyl)benzoyloxy) biphenylcarbonyloxy)butane-1,4-diyl bis(4'-(4-(allyloxy)benzoyloxy) biphenyl-4-carboxylate) (BTA2) and butane-1,2,4-triyl tris(4'-(4-(allyloxy)benzoyloxy) biphenyl-4-carboxylate) (BTA3) are shown in Scheme 2 and the details of the experiment are summarized in Table 1. BTA0 and BTA3 are symmetric three-arm LCs (**TALCs**). BTA1 and BTA2 are asymmetric **TALCs**.

The symmetric three-arm LCs, BTA0 and BTA3, have been synthesised by the one-step reaction between O-H groups of BT and aromatic acid of the LC side arms in THF and pyridine toluene, using DCC and DMAP as catalyst. The synthesis of BTA0 is given as a representative example.

A solution of 1,2,4-butanetriol (BT, 0.318g, 3mmol) and pyridine (15mL) were placed into a 100mL round flask. A solution of *N,N'*-dicyclohexyl carbodiimide (DCC, 1.86g, 9mmol), 4-dimethylamino pyridine (DMAP, 0.55g) and THF (20mL) was put into the flask. A sample of TFBA (3.48g, 9mmol) was dissolved in 60mL pyridine and then put them into the flask, too. The mixture was stirred at 40°C until the result of FTIR analysis showed that the characteristic absorption band of C=N (2117 cm⁻¹) disappeared completely. The 1,3-dicyclohexylurea (DCU) was separated from the reaction mixture by filtration for several times. The filtrate was concentrated and then poured into water. The water solution was neutralized with dilute hydrochloric acid. The crude product was obtained by filtration and washed with

water. The white powder of BTA0 was obtained after several re-crystallization from ethyl ether. Yield: 48%. M.p.: 118.0°C. Elemental analysis calculated for C₆₇H₄₃F₉O₁₂: C, 66.45; H, 3.58; F, 14.12; O, 15.85%. Found: C, 66.41; H, 3.61; F, 14.10; O, 15.88%.

IR (KBr, cm⁻¹): 2997-2850 (C - H), 1738, 1711 (C = O), 1609, 1496 (Ar), 1123 (C - F).

¹H NMR (CDCl₃, TMS, δ): 2.110-2.210 (m, 2H, -CH₂-), 4.190-4.455 (m, 5H, -CH₂-, ^HC<), 7.330-7.340(m, 6H, Ar - H), 7.660-7.670(m, 6H, Ar - H), 7.690-7.710 (m, 6H, Ar - H), 7.820-7.834 (d, *J* = 8.4 Hz, 6H, Ar - H), 8.147-8.161(m, 6H, Ar - H), 8.365-8.379 (d, *J* = 8.4 Hz, 6H, Ar - H).

For the synthesis of asymmetric TALCs, BTA1 and BTA2, regioselectivity should be considered. The activity of the three hydroxyl groups of BT is different. The activity of the two primary hydroxyl groups of BT is stronger than that of the secondary hydroxyl groups. That the different side arms reacting with BT simultaneously will result in the generation of the isomers. Their properties and spectra are similar. It is difficult to separate them. So the key is to reduce the generation of the isomers as much as possible. The measures of two-step method and adding the solution of the LC side arm dropwise to the reactive system were adopted for the synthesis of asymmetric **TALCs**. These measures can decrease the generation of the isomers. The synthesis of BTA1 is given as a representative example of the two-step method.

A solution of BT (0.318g, 3mmol) and 10mL pyridine and 15mL THF were placed

into a 100mL round flask. A solution of DCC (1.86g, 9mmol), DMAP (0.55g) and THF (20mL) was put into the flask. A sample of TFBA (2.32g, 6mmol) was dissolved in 50mL THF. The solution of TFBA was added dropwise into the BT solution for about 12 h. The reaction mixture was stirred at 40°C until the result of FTIR analysis showed that the characteristic absorption bands of carboxylic acid disappeared completely. A sample of AOBA (1.12g, 3mmol) was dissolved in 30mL THF. The solution of AOBA was added into the above reaction mixture. The reaction mixture was stirred at 40°C until the result of FTIR analysis showed that the characteristic absorption bands of C=N (2117cm⁻¹) disappeared completely. The DCU was separated from the reaction mixture by filtration for several times. The filtrate was concentrated and then poured into water. The water solution was neutralized with dilute hydrochloric acid. The crude product was obtained by filtration and washed with water. The white powder of BTA1 was obtained after several re-crystallization from ethyl ether. Yield: 40%. m.p.: 63.8°C. Elemental analysis. Calculated for C₆₉H₄₈F₆O₁₃: C, 69.11; H, 4.03; F, 9.51; O, 17.35%. Found: C, 69.06; H, 4.11; F, 9.46; O, 17.37%.

IR (KBr, cm⁻¹): 2955-2854 (C - H), 1736, 1713 (C = O), 1606,1492 (Ar), 1123 (C - F).

¹H NMR (CDCl₃, TMS, δ) 2.186-2.204 (m, 2H, -CH₂-), 4.126-4.137 (m, 2H, -CH₂O-), 4.314-4.371 (m, 1H, $\overset{\text{H}}{\text{C}}\text{<}$), 4.404-4.474 (m, 2H, -CH₂O-), 4.650-4.687 (m, 2H, -CH₂O), 5.347-5.364 (d, *J* = 10.2, 1H, =CH₂), 5.449-5.480 (d, *J* = 18.6, 1H, =CH₂), 6.056-6.111 (m, 1H, -CH=), 7.239-7.241(d, *J* = 1.2 Hz, 2H, Ar - H), 7.339-

7.358 (dd, $J_1 = 2.7$ Hz, $J_2 = 6.0$ Hz, 6H, Ar - H), 7.677-7.691 (m, 6H, Ar - H), 7.700-7.715 (d, $J = 9.0$ Hz, 4H, Ar - H), 7.808-7.821 (d, $J = 7.8$ Hz, 6H, Ar - H), 8.121-8.148 (m, 8H, Ar-H), 8.352-8.366 (d, $J = 8.4$ Hz, 4H, Ar - H).

3. Results and discussion

3.1. Structural characterization

Chemical structures of TFBA, AOBA and the **TALCs** were characterized with FTIR, elemental analysis and ^1H NMR spectra. In the ^1H NMR spectra of TFBA, AOBA and **TALCs**, the peaks with chemical shifts 2.110-2.210 and 4.120-4.687 ppm correspond to alkyl protons, and 5.349-6.115 and 7.018-8.366 ppm correspond to olefinic protons and aromatic protons, respectively. The IR spectra of TFBA, AOBA and **TALCs** contained characteristic peaks near 3070-2544 cm^{-1} associated with stretching band of hydroxyl groups in carboxylic acid dimers, strong peaks near 1739 and 1729 cm^{-1} corresponding to C=O in ester, and the strong peaks near 1685 cm^{-1} corresponding to C=O in carboxylic acid dimers. The results of FT-IR, elemental analysis and ^1H NMR spectroscopy of TFBA, AOBA and **TALCs** were in good agreement with the anticipated structures.

1,2,4 - Butanetriol (*BT*) is a kind of chiral molecule which has three hydroxyl groups. The specific rotation of *BT* (in THF) is -2.9° . The **TALCs** (in THF) exhibited optical active, too. The **TALCs**' specific rotations were given in Table 1. It is obvious that the chiral core played an important role in the **TALCs**' optical active. An interesting phenomenon is that the **TALCs**' specific rotations are greater than their chiral core. This may be attributed to that larger steric effect of the **TALCs** hindered

the free rotation of single bond of C-C and C-O in the *BT*, which resulted in one of the two optical isomers increasing.

3.2. Liquid crystal properties of LC arms

The liquid crystalline behavior of the LC side arms TFBA and AOBA was studied using DSC, POM and XRD. TFBA and AOBA exhibited thermotropic mesomorphic behavior. The transition temperatures and associated enthalpy changes seen for TFBA and AOBA are summarized in Table 2, and the DSC thermograms are displayed in Fig.1, Fig.2, Fig.3, and Fig.4.

TFBA displayed liquid crystal phase at about 253.5°C on heating. The sample displayed no LC - isotropic transition but solidification and carbonization when the sample was heated further. Liquid crystal phase was not observed in the subsequent cooling. There are two phase transition at 253.5°C and 291.2°C in the DSC heating curve of TFBA (see Fig.1). There was not any phase transition in the DSC curve on cooling. DSC and POM studies indicated that the melting temperature of TFBA is 253.5°C. The TGA result helped us to get a better understanding of the thermal properties and mesomorphic properties of TFBA. TGA result (see Fig. 1) indicated that 3.7% and 31% weight loss occurred at 291.2°C and 350°C, respectively. The obvious decomposition may destroy the structure of TFBA. This may be the cause that there was no phase transition and liquid crystal phase being observed in the subsequent cooling process. While TFBA still displayed mesomorphic properties at $T_{2\%}$ (271.6°C, the temperature at which 2% mass loss occurred in TGA). So $T_{2\%}$ was adopted as the final temperature of the mesophase in the present study.

TFBA was heated to 271.6°C and then cooled to study its thermal properties and mesomorphic phase on cooling. In the subsequent cooling process, the liquid crystal phase was observed by POM and the sample crystallized at about 203°C. The DSC curve of TFBA shows crystallization at 203.9°C on cooling, too. (see Fig.2).

The results of DSC and POM indicated that TFBA was a thermotropic enantiotropic LC. It shows a melting transition at 253.5°C, the temperature at which 2% weight loss occurred is 271.6°C and the mesomorphic region (ΔT_1) is about 18.1°C on first heating (The mesomorphic region on heating cycle is to be calculated in this way: 271.6-253.5=18.1°C). While on cooling, crystallization occurred at 203.9°C. The mesomorphic region (ΔT_2) is about 67.7°C. (The mesomorphic region on cooling cycle is to be calculated in this way: 271.6-203.9=67.7°C).

Fig. 3 shows only one phase transition at 198.7°C on heating for AOBA and there is not any phase transition in the DSC curve on cooling. When AOBA was heated, the sample melt at about 198°C. The sample displayed no LC - isotropic transition but solidification and carbonization when the sample was heated further. Liquid crystal phase was not observed in the subsequent cooling. Also the TGA result helped us to get a better understanding of the thermal properties and mesomorphic properties of AOBA. Fig. 3 indicated that the sample lost 3% weight at 300.0°C. The decomposition may destroy AOBA's structure. This may be the cause that the LC phase solidified and the sample carbonized after AOBA being heated to 300°C. It is also the reason for no LC phase being observed in the subsequent cooling process. $T_{2\%}$ (291.0°C) was adopted as the final temperature of AOBA's mesophase in the

present study (AOBA still displayed mesomorphic properties at 291.0°C).

AOBA was heated to not too high but only 260.0°C and then cooled to study the cooling process' thermal properties and mesomorphic phase. The liquid crystal phase was observed by POM and the sample crystallized at about 193°C in the subsequent cooling process. Fig. 4 shows that AOBA crystallized at 193.7°C on cooling.

The results of DSC and POM indicated that AOBA is a thermotropic enantiotropic LC. It showed a melting endotherm at 198.7°C, the temperature at which 2% weight loss occurred is 291.0°C and the mesomorphic region (ΔT_1) is about 92.3°C on heating, as well as LC–crystal transition is at 193.7°C and the mesomorphic region (ΔT_2) is about 97.3°C on cooling (The calculating method of the mesomorphic regions is similar with that of TFBA) .

TFBA exhibited mosaic texture on heating and cooling cycle (see Fig. 5a). A variable-temperature X-ray diffraction study was carried out on TFBA to obtain more detailed information on its LC phase structure. Fig. 6 shows the X-ray patterns at different temperature (260°C and 270°C) within TFBA's liquid crystal rang. The sharp peaks at $2\theta = 3.0$ ($d = 29.41 \text{ \AA}$) seen at different temperature indicated that layer spacing was independent of temperature. The molecular length L of TFBA is estimated to be 15.6 Å, while that of the dimer of TFBA is estimated to be 28.6 Å, and approximately equals to the smectic layer spacing, suggesting that the molecular arrangement is in the form of dimmers and the director n is perpendicular to the smectic layer plane. The results of the X-ray and mosaic texture of TFBA suggested

that it is a smectic B (S_mB) LC. AOBA exhibited thread-like texture on heating and cooling cycle. Thread-like texture is typical texture of nematic. The results of DSC and POM indicated that AOBA is a nematic (N) LC.

The chemical structure of TFBA and AOBA is somewhat similar. The two LC arms all have the structure of 4' - (benzoyloxy) biphenyl - 4 - carboxylic acid. The difference between them is the terminal group. The terminal group of AOBA is allyloxy, while the terminal group of TFBA is trifluoromethyl. In general, fluorine's strong electronegativity results in a strongly polar C-F bond. The stronger polarity of terminal trifluoromethyl group may increase the anisotropy of the molecule, and result in an increase of the inter-molecular forces. This may be the cause that the melting temperature of TFBA is 54.8°C higher than that of AOBA.

3.2. Liquid crystal properties of TALCs

The thermal properties and phase behavior of TALCs (BTA0, BTA1, BTA2 and BTA3) were investigated with DSC. The phase-transition temperatures and corresponding enthalpy changes of the TALCs obtained on the first heating and cooling cycle were summarized in Table 2, and the DSC curves are presented in Fig. 7, Fig.8, Fig.9 and Fig.10. The exothermic peaks of crystallization of BTA0 - BTA3 are not obvious and some of them even have not been observed. This may be due to their dendritic structures. In general, the dendritic material is not easy to crystallize. In this study, the temperatures of crystallization of some TALCs were obtained from POM.

DSC curves of BTA0 show a melting endotherm at 118.0°C ($\Delta H=27.24 \text{ J g}^{-1}$) and a chiral smectic C (S_mC^*) - isotropic (I) phase transition at 201.0°C ($\Delta H=2.28 \text{ J g}^{-1}$)

g^{-1}) on heating, as well as $I - \text{SmC}^*$ transition at 181.0°C ($\Delta H = -3.05 \text{ J g}^{-1}$) and crystallization at 95.2°C ($\Delta H = -11.4 \text{ J g}^{-1}$) on cooling. DSC curves of BTA1 show a melting endotherm at 63.8°C ($\Delta H = 0.70 \text{ J g}^{-1}$), a chiral smectic A (S_mA^*) - cholesteric (ch) phase transition at 92.5°C ($\Delta H = 0.78 \text{ J g}^{-1}$) and $ch - I$ phase transition at 163.2°C ($\Delta H = 0.43 \text{ J g}^{-1}$) on heating, as well as $I - ch$ transition at 156.1°C ($\Delta H = -0.08 \text{ J g}^{-1}$) and $ch - \text{S}_m\text{A}^*$ transition at 142.5°C ($\Delta H = -0.20 \text{ J g}^{-1}$). The exothermic peak of crystallization of BTA1 has not been observed on DSC's cooling curve. The transition temperature of chiral smectic A to crystal phase (54.5°C) of BTA1 on Table 2 was obtained by POM. DSC curves of BTA2 show a melting endotherm at 101.1°C ($\Delta H = 2.61 \text{ J g}^{-1}$) and $ch - I$ phase transition at 222.6°C ($\Delta H = 0.48 \text{ J g}^{-1}$) on heating, as well as $I - ch$ transition at 222.1°C ($\Delta H = -0.18 \text{ J g}^{-1}$) and crystallization at 73.9°C ($\Delta H = -0.21 \text{ J g}^{-1}$) on cooling. DSC curves of BTA3 show a melting endotherm at 90.4°C ($\Delta H = 8.10 \text{ J g}^{-1}$) and $ch - I$ phase transition at 217.6°C ($\Delta H = 3.20 \text{ J g}^{-1}$) on heating, as well as $I - ch$ transition at 213.9°C ($\Delta H = -0.25 \text{ J g}^{-1}$) on cooling. The exothermic peak of crystallization of BTA3 has not been observed on cooling cycle on DSC curve. The transition temperature of cholesteric to crystal phase (60.5°C) of BTA3 on Table 2 was obtained from POM, too.

The melting temperatures of **TALCs** (BTA0 - BTA3) are lower than those of the LC side arms. This may be due to their different structure. The structure of the LC side arms (TFBA and AOBA) is aromatic acid. The hydrogen bond of aromatic acid makes the LC side arms have higher melting temperature. In addition, the lower melting temperature of **TALCs** may be attributed to their dendritic structures. The

mesomorphic regions of **TALCs** (see Fig.11) are wider than those of the corresponding LC side arms. This may be attributed to the lower melting temperatures and the lower temperatures of crystallization of **TALCs**. Fig. 11 shows that the mesomorphic regions increase gradually from BTA0 to BTA3 on heating and cooling. This may be attributed to the increase of the content of AOBA, which has wider mesomorphic region.

Fig. 12a - Fig. 12j show **TALCs**' characteristic textures. BTA0 displayed thermal enantiotropic chiral smectic C (S_C^*) texture. When BTA0 was heated, the broken fan-shaped texture appeared (see Fig. 12(a)). The texture did not disappear until the sample became isotropic. The droplet texture separated from the isotropic melt at about 181°C on cooling. As the sample was cooled further, the droplets gradually aggregated to form a broken fan-shaped texture with striations due to the helical superstructure (see Fig. 12(b)). The broken fan-shaped texture did not disappear until the sample crystallized. BTA1 displayed thermal enantiotropic S_mA^* and cholesteric textures on heating and cooling. When BTA1 was heated to about 63°C, focal-conic texture appeared at first, and then there was a subtle change and broken fan-shaped texture displayed. The texture did not disappear until the sample became isotropic. The fan-shaped texture appeared at first on cooling (see Fig. 12 (c)). There was also a subtle change as the sample was cooled further. The fan-shaped texture changed into focal-conic texture (see Fig. 12(d)). The focal-conic texture did not disappear until the sample crystallized. BTA2 displayed thermal enantiotropic cholesteric textures on heating and cooling. When BTA2 was heated, the sample melted and catenoid

birefringent region containing small fan-shaped texture appeared (see Fig. 12 (e)). As the sample was heated further, fingerprint texture appeared (see Fig. 12 (f)) and did not disappear until the sample became isotropic. The cholesteric droplet texture separated from the isotropic melt on cooling (see Fig. 12 (g)). The cholesteric droplet texture did not disappear until the sample crystallized. BTA3 displayed thermal enantiotropic cholesteric textures on heating and cooling. When BTA3 was heated, the sample melted and focal-conic texture appeared at first (see Fig. 12 (h)) and then gradually changed into fingerprint texture (see Fig. 12 (i)). Fingerprint texture did not disappear until the sample became isotropic. As the sample was cooled, the cholesteric droplet texture separated from the isotropic melt at about 214°C and did not disappear (see Fig. 12 (j)) until the sample crystallized.

The fan-shaped or focal conic textures are preferably observed in rather thin sample preparations in S_mA phase. From a texture point of view, the S_mA and the S_mA^* phases are equivalent in appearance. It is used to distinguish the S_mA and the S_mA^* phases whether the LC displays optical active. An often observed S_mC^* appearance is that of the so-called broken fan-shaped texture. This formation of a helical superstructure in chiral bulk S_mC^* samples makes it easy to detect the S_mA^* and S_mC^* . In S_mA^* , the backs of the fans of focal conic or fan-shaped textures appear smooth, the occurrence of an arced equidistant line pattern indicates the mesophase is S_mC^* .

Fingerprint texture is a typical texture of cholesteric phase, and fan-shaped texture is often observed in cholesteric phase, too. But the orientation of the helix axis

in them is different. For fingerprint texture, the twist axis lies in the plane of the substrate, within the substrate plane there is no preferred direction, and thus the direction of the twist axis is allowed to vary smoothly over macroscopic distances. The varying director field leads to an equidistant pattern of dark lines, which is called a fingerprint texture. Dark stripes appear, whenever the local director is oriented along the direction of light propagation, i. e. at vanishing birefringence. While for fan-shaped texture, the twist axis naturally deviates from the substrate normal. Fan-shaped textures of cholesteric phase are very similar to those observed in S_mA phases. The cholesteric fan-like textures are observed for strongly twisted materials, while fan-shaped textures that exhibit focal conics are found for materials with a slightly smaller twist. Especially the latter textures are very similar to that of the S_mA phase, but with a somewhat smoother appearance of the fans. [34]

The variable-temperature X-ray diffraction study was carried out on BTA0 - BTA3 to obtain more detailed information on its LC phase structure. Fig. 13(a) shows the X-ray patterns at different temperature within BTA0's liquid crystal rang. The sharp peaks at $2\theta = 3.3^\circ$ (strong) and $2\theta = 7.0^\circ$ (weak), corresponding to $d = 26.74 \text{ \AA}$, $d = 12.61 \text{ \AA}$, respectively, were observed at 135°C on heating. The sharp peaks at $2\theta = 2.3^\circ$ (strong), $2\theta = 3.9^\circ$ (weak) and 7.6° (very weak), corresponding to $d = 38.37 \text{ \AA}$, $d = 22.63 \text{ \AA}$ and $d = 11.77 \text{ \AA}$, respectively, were observed at 160°C on heating. The diffuse peaks at about $2\theta = 19.0^\circ$, corresponding to molecular lateral spacing, were observed at the two temperatures.

Fig. 13(b) shows the X-ray patterns on different temperature within BTA1's liquid

crystal rang on cooling. Only the diffuse peak $2\theta = 18.0^\circ$ was observed for BTA1 at 150°C . Within the S_mA^* mesomorphic region, the sharp peaks at $2\theta = 3.5^\circ$ (strong), $2\theta = 7.1^\circ$ (weak) and 10.7° (very weak), corresponding to $d = 25.21 \text{ \AA}$, $d = 12.44 \text{ \AA}$ and $d = 8.26 \text{ \AA}$, respectively, were observed at 120°C and 100°C . The diffuse peaks at about $2\theta = 18.0^\circ - 19.0^\circ$, which corresponding to the molecular lateral spacing of BTA1, were observed at 120°C and 100°C , too.

Fig. 13(c) and Fig. (d) show the X-ray patterns at different temperature on heating within LC rang of BTA2 and BTA3, respectively. Only diffuse peak at about $2\theta = 18.0^\circ - 19.0^\circ$ was observed for BTA2 and BTA3. These were consistent with their optical textures, suggesting that BTA2 and BTA3 are cholesteric LCs.

That the location of the sharp peaks of BTA0 changed at different temperature indicated that the layer space depended on temperature. For S_mC , the tilt angle θ increases with decreasing temperature and thus the smectic layer spacing decreases with decreasing temperature. The situation of BTA0 that the tilt θ increased with decreasing temperature is consistent with that of S_mC . We also noticed that the intensity of the sharp peaks at 160°C was much greater than that at 135°C , suggesting that the degree of long-range ordering of BTA0 increased with increasing temperature. The cause of this may be due to the fact that the molecular mobility of BTA0 increased with increasing temperature, providing help to the LC molecules in forming an ordered lamellar arrangement.

The X-ray patterns of BTA0 and BTA1 displayed the sharp peaks at different angle at a certain temperature within their LC rang, for example, BTA1 displayed

sharp peaks at $2\theta = 3.5^\circ$, 7.1° , 10.7° . The sharp peaks appeared at different angles indicated the existence of layers of different thickness ($d = 25.21 \text{ \AA}$, $d = 12.44 \text{ \AA}$ and $d = 8.26 \text{ \AA}$, respectively). Star-shaped LC molecule is different from rod-like LC molecule, whose side arms extend to space as far as possible. Fig. 14 is the 3D molecular model of BTA1. Fig. 14 (A) is the front view and Fig. 14 (B) is the side view. Fig. 14 displayed that the height, width and length of BTA1 molecule are 21.37 \AA , 8.57 \AA and 11.95 \AA , respectively. When these molecules arrange in layers, the long range order with different thickness is formed (see Fig. 15). This may be the cause for that different sharp peaks were observed. That the difference between BTA1's layer thickness measured by X-ray (25.21 \AA , 12.44 \AA and 8.26 \AA) and its height, width and length calculated (21.37 \AA , 8.57 \AA and 11.95 \AA) is not much, which confirmed our conjecture in a certain degree. The intensity of the sharp peak at $2\theta = 3.5^\circ$ is much stronger than that at $2\theta = 7.1^\circ$ or 10.7° , indicating that long range order in a certain direction dominated.

BTA1's XRD results at 120°C and 100°C (within the S_mA^* mesomorphic region) indicated that the layer space was independent of temperature. This may be due to that the director n and the optic axis are perpendicular to the smectic layer plane in the S_mA^* phase. The intensity of the sharp peaks at $2\theta = 3.5^\circ$, 7.1° and 10.7° increased with the temperature decreasing from 120°C to 100°C , suggesting that the lamellar structure perfected with decreasing temperature. BTA1's XRD results were consistent with its optical textures, suggesting that BTA1 is S_mA^* LC at the lower temperature mesomorphic region and cholesteric LC at the higher temperature mesomorphic

region.

We noticed that chiral core and the mesomorphic type of the two LC side arms played important effects on the mesomorphic type of the **TALCs** in this study. The **TALCs** displayed chiral properties affected by the chiral core, but their mesomorphic types were affected by the mesomorphic types of the LC side arms. The **TALC** BTA3 displayed cholesteric phase. The result is similar to the previous studies [23-25], which chiral core is prone to induce the cholesteric phase in the multi-arm LCs with nematic side arms. The only difference is that the nematic LC side arms were introduced into the chiral core by flexible spacer in previous studies, while in this study, the rigid nematic LC side arm was introduced into the chiral core directly, without flexible spacer. The **TALC** BTA0, with three S_mB side arms, displayed S_C^* . The result indicated that the chiral core made the **TALC** display chiral property but the dendritic structure reduced the degree of order of the lamellar liquid crystal. BTA1 and BTA2 with both the nematic LC side arm and the smectic LC side arm in them also displayed chiral properties. The introduction of the nematic LC side arm made the **TALCs** (BTA1, BTA2 and BTA3) be prone to display cholesteric phase.

4. Conclusion

A series of symmetric and asymmetric three-arm liquid crystals (**TALCs**) with 1, 2, 4 - butanetriol as chiral core and 4' - (4 - (trifluoromethyl) benzoyloxy) biphenyl- 4 - carboxylic acid (TFBA) and 4' - (4 - (allyloxy) benzoyloxy) biphenyl - 4 - carboxylic acid (AOBA) as LC side arms have been synthesised. The influence on **TALCs** properties played by the chiral core and the nature of the LC side arms have been

studied. TFBA is a smectic B LC, while AOBA is a nematic LC. Compared to TFBA, the melting temperature of AOBA is lower and its mesophase temperature range is wider. The **TALC** BTA0 exhibited chiral smectic C, while BTA1, BTA2 and BTA3 displayed cholesteric phase, in addition BTA1 displayed chiral smectic A at the lower temperature of the mesophase temperature range. The introduction of chiral core into **TALCs** makes both the symmetric and the asymmetric **TALCs** display chiral properties. The absolute values of specific rotation of the **TALCs** are bigger than that of the chiral core. Compared to the S_mB LC side arm (TFBA), the degrees of order of the **TALCs** (BTA0 - BTA2, with TFBA in them) are reduced and this can be attributed to their dendritic structure. The introduction of the nematic LC side arm made the **TALCs** (BTA1, BTA2 and BTA3) be prone to display cholesteric phase. The melting temperatures of **TALCs** are lower than those of the corresponding LC side arms, while their mesophase temperature ranges are wider. The mesomorphic regions increased gradually from BTA0 to BTA3 on heating and cooling.

Acknowledgements

This work was financially supported by the Fundamental Research Funds for the Central Universities (N130205001), Science and Technology Bureau of Shenyang (F14-231-1-05) and the National Natural Science Fund of China (51273035).

ReferencesReferences

- [1] D.J. Broer, J. Lub, G.N. Mol, Nature. 378 (1995) 467-469.
- [2] M. Brehmer, J. Lub, P. van de Witte, Adv. Mater. 10 (1998) 1438-1441.
- [3] M.M. Green, N.C. Peterson, T. Sato, A. Teramoto, R. Cook, S. Lifson, Science.

268 (1995) 1860-1866.

[4] V. I. Kopp, B. Fan, H.K.M. Vithana, A.Z. Genack, *Opt. Lett.* 23 (1998) 1707-1709.

[5] Y.C. Yang, C.S. Kee, J.E. Kim, H.Y. Park, J.C. Lee, Y.J. Jeon, *Phys. Rev. E.* 60 (1999) 6852-6854.

[6] H. Finkelmann, S.T. Kim, A. Munoz, P. Palffy-Muhoray, B. Taheri, *Adv. Mater.* 13 (2001) 1069-1072.

[7] J. Xiang, Y. Li, Q. Li, D.A. Paterson, J.M.D. Storey, C.T. Imrie, O.D. Lavrentovich, *Adv. Mater.* 27 (2015) 3014-3018.

[8] Y. Jin, Z. Hong, S.B. Kwon, *Journal of the Society for Information Display.* 22 (2015) 581-587.

[9] B.G. Kim, S. Kim, S.Y. Park, *Tetrahedron Lett.* 42 (2001) 2697-2699.

[10] M. Lehmann, R.I. Gearba, M.H.J. Koch, D.A. Ivanov, *Chem. Mater.* 16 (2004) 374-376.

[11] H. Meier, M. Lehmann, H.C. Holst, D. Schwoppe, *Tetrahedron.* 60 (2004) 6881-6888.

[12] Y. H. Ooi, G.Y. Yeap, D. Takeuchi, *J. Mol. Struct.* 1051 (2013) 361-375.

[13] M. Lehmann, M. Jahr, B. Donnio, R. Graf, S. Gemming and I. Popov, *Chem. Eur. J.* 14 (2008) 3562-3576.

[14] D.S. Yao, B.Y. Zhang, Y.H. Li, W.Q. Xiao, *Tetrahedron Lett.* 45 (2004) 8953-8956.

[15] D.S. Yao, B.Y. Zhang, W.W. Zhang, M. Tian, *J. Mol. Struct.* 881 (2008) 83-89.

[16] B.Y. Zhang, D.S. Yao, F.B. Meng, Y.H. Li, *J. Mol. Struct.* 741 (2005) 135-140.

- [17] B.Y. Zhang, W.Q. Xiao, Y.H. Cong, Y.H. Zhang, *Liq. Cryst.* 34 (2007) 1129-1136.
- [18] S.K. Pal, S. Setia, B.S. Avinash, S.Kumar, *Liq. Cryst.* 40 (2013) 1769-1816.
- [19] M. Lehmann, M. Jahr, F.C. Grozema, R.D. Abellon, L.D.A. Siebbeles, and M. Müller, *Adv Mater.* 20 (2008) 4414-4418.
- [20] J.H. Lee, H.J. Lee, S.J. Lee, J. Jang, S.H. Yoo, J.Y. Jho, *Liq. Cryst.* 40 (2013) 112-119.
- [21] S.J. Lee, M.K. You, S.W. Lee, J. Lee, J.H. Lee, J.Y. Jho, *Liq. Cryst.* 38 (2011) 1289-1299.
- [22] I.M. Saez, J.W. Goodby, *Chem. Eur. J.* 9 (2003) 4869-4877.
- [23] M. Tian, B.Y. Zhang, Y.H. Cong, N. Zhang, D.S. Yao, *J. Mol. Struct.* 923 (2009) 39-44.
- [24] M. Tian, B.Y. Zhang, Y.H. Cong, B. Zhang, *J. Mol. Struct.* 937 (2009) 131-135.
- [25] M. Tian, B.Y. Zhang, Y.H. Cong, X.Z. He, H.S. Chu, X.Y. Zhang, *Liq. Cryst.* 37 (2010) 1373-1379.
- [26] M. Hird, *Chem. Soc. Rev.* 36 (2007) 2070-2095.
- [27] M. Tian, H.H. Sun, X.W. Tian, Z.X. Xu, F.Q. Wang, D.S. Yao, J.S. Hu, *Liq. Cryst.* 42 (2015) 298-308.
- [28] F.B. Meng, Z.Y. Wang, G.W. Chai, H.G. Wang, Y. Chen, B.Y. Zhang, *J. App. Poly. Sci.* 116 (2010) 2384-2395.
- [29] G.W. Skelton, P. Brett, J.C. Jones, S.M. Kelly, V. Minter, R.P. Tuffin, *Liq. Cryst.* 28 (2001) 417-435.

- [30] T. Tasaka, S. Takenaka, K. Kabu, Y. Morita, H. Okamoto, *Ferroelectrics*. 276 (2002) 83-92.
- [31] G.H. Hsiue, L.H. Wu, C.J. Hsieh, R.J. Jeng, *Liq. Cryst.* 19 (1995) 189-195.
- [32] W. Drzewinski, K. Czuprynski, R. Dabrowski, J. Przedmojski, M. Neubert, S. Yakovenko, A. Muravski, *Mol. Cryst. Liq. Cryst.* 351 (2000) 297-304.
- [33] G.P.C. Chien, J.F. Kuo, C.Y. Chen, *J. Polym. Part A: Sci. Polym. Chem.* 31 (1993) 2423-2436.
- [34] I. Dierking, In *Die Deutsche Bibliothek, Textures of Liquid Crystal*, WILEY-VCH Verlag, Weinheim, 2003 (56–101).

Table 1. Inventory ratio, Specific Rotation of the three-arm liquid crystals

| sample | Feed/mmol | | | specific Rotation (°) |
|--------|---------------|-----------------|-----------------|--------------------------|
| | <i>n</i> (BT) | <i>n</i> (TFBA) | <i>n</i> (AOBA) | |
| BTA0 | 3 | 9 | 0 | +18.60 |
| BTA1 | 3 | 6 | 3 | +7.78 |
| BTA2 | 3 | 3 | 6 | -5.54 |
| BTA3 | 3 | 0 | 9 | -8.30 |

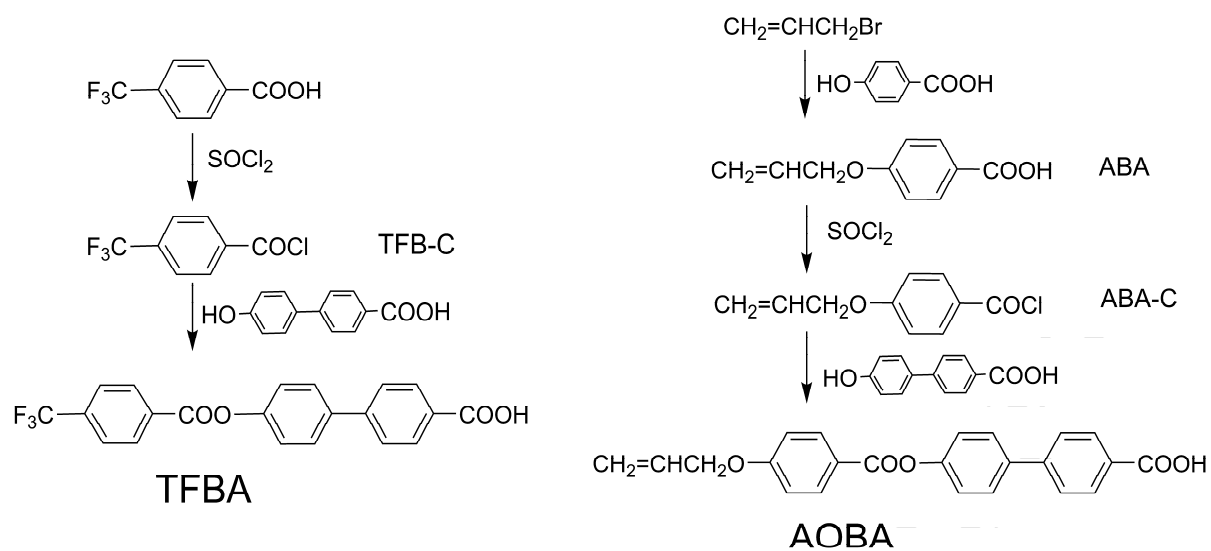
Table 2. Phase transitions, phase transition enthalpies and mesogenic range for LC side arms and the three - arm LCs.

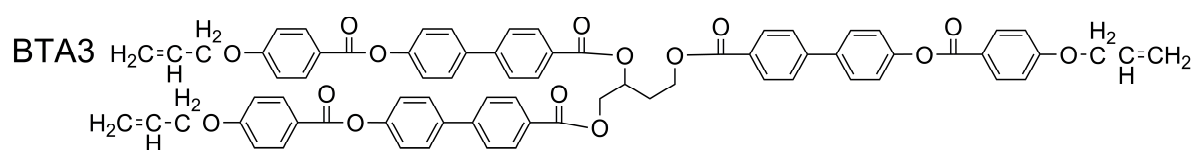
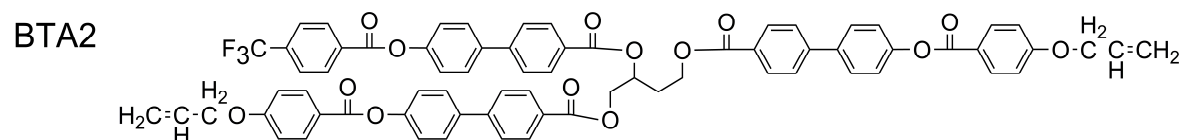
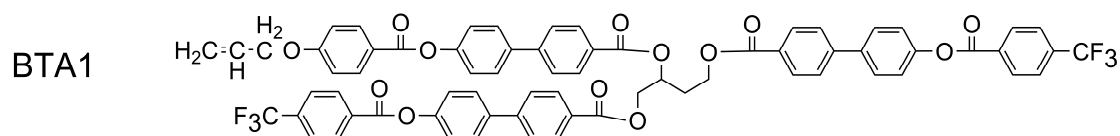
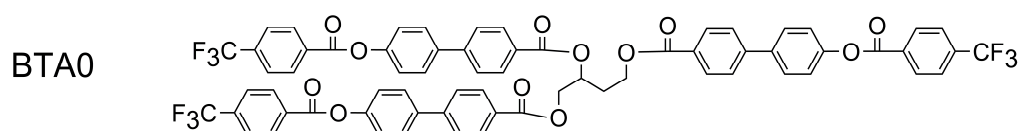
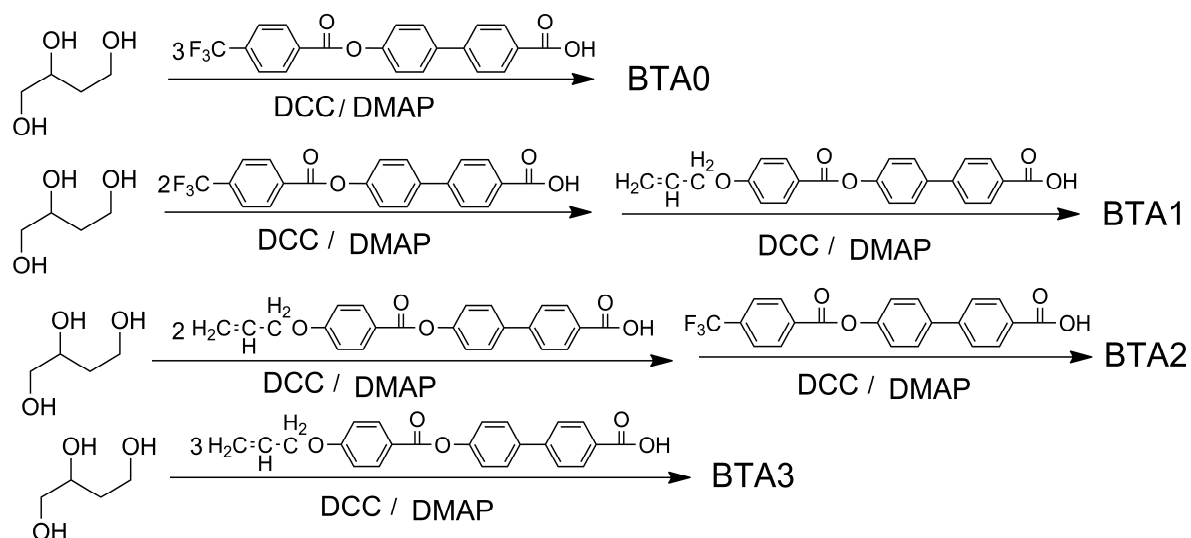
| Sample | Phase transitions, °C (corresponding enthalpy changes, J/g) ^a | ΔT , °C | Meso-phase |
|--------|--|-----------------|------------------------|
| TFBA | heating: Cr 253.5 (10.60) S _m B 271.6 ^b (-) I | 18.1 | S _m B |
| | cooling: Cr 203.9 (-4.77) S _m B 271.6 ^b (-) I | 67.7 | |
| AOBA | heating: Cr 198.7 (48.06) N 291.0 ^b (-) I | 92.3 | N |
| | cooling: Cr 193.7 (-5.29) N 291.0 ^b (-) I | 97.3 | |
| BTA0 | heating: Cr 118.0 (27.24) S _m C* 201.0 (2.28) I | 83.0 | S _m C* |
| | cooling: Cr 95.2 (-11.40) S _m C* 181.0 (-3.05) I | 85.8 | |
| BTA1 | heating: Cr 63.8 (0.70) S _m A* 92.5 (0.78) ch 163.2 (0.43) I | 99.4 | S _m A* - ch |
| | cooling: Cr 54.5 ^c (-) S _m A* 142.5 (-0.20) ch 156.1 (-0.08) I | 101.6 | |
| BTA2 | heating: Cr 101.1 (2.61) ch 222.6 (0.48) I | 121.5 | ch |
| | cooling: Cr 73.9 (-0.21) ch 222.1 (-0.18) I | 148.2 | |
| BTA3 | heating: Cr 90.4 (8.10) ch 217.6 (3.20) I | 127.2 | ch |
| | cooling: Cr 60.5 ^c (-) ch 213.9 (-0.25) I | 153.4 | |

^aCr, crystalline phase; S_mB, smectic B; S_mC*, chiral smectic C; S_mA*, chiral smectic A; ch, cholesteric; I, isotropic phase.

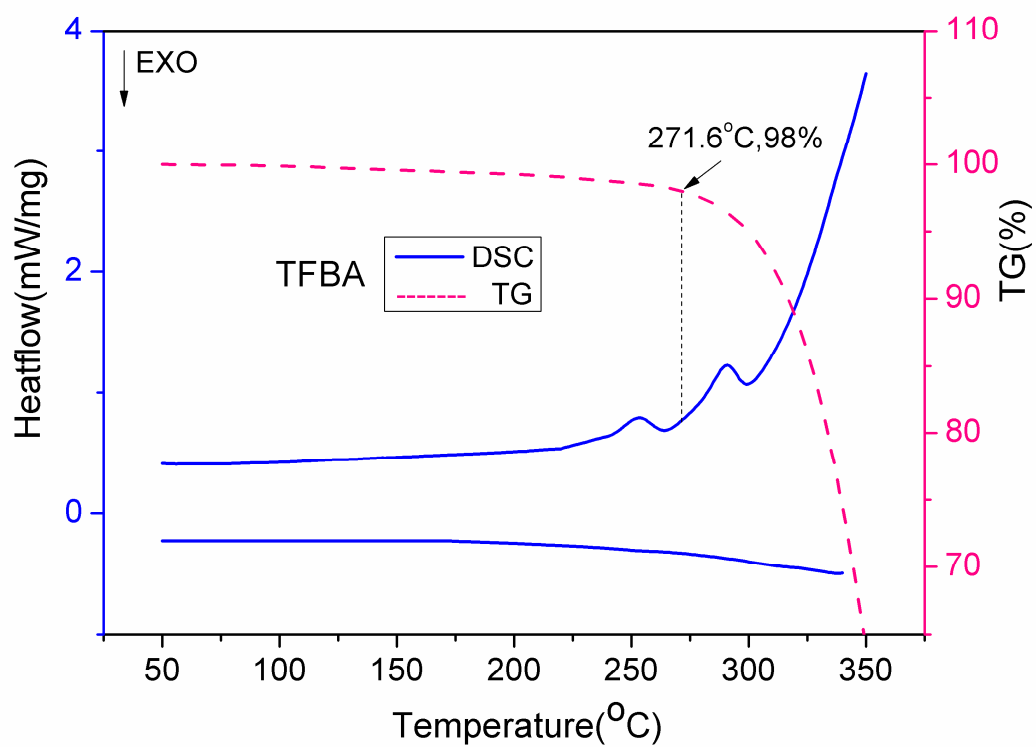
^bthe temperature at which 2% weight loss occurs.

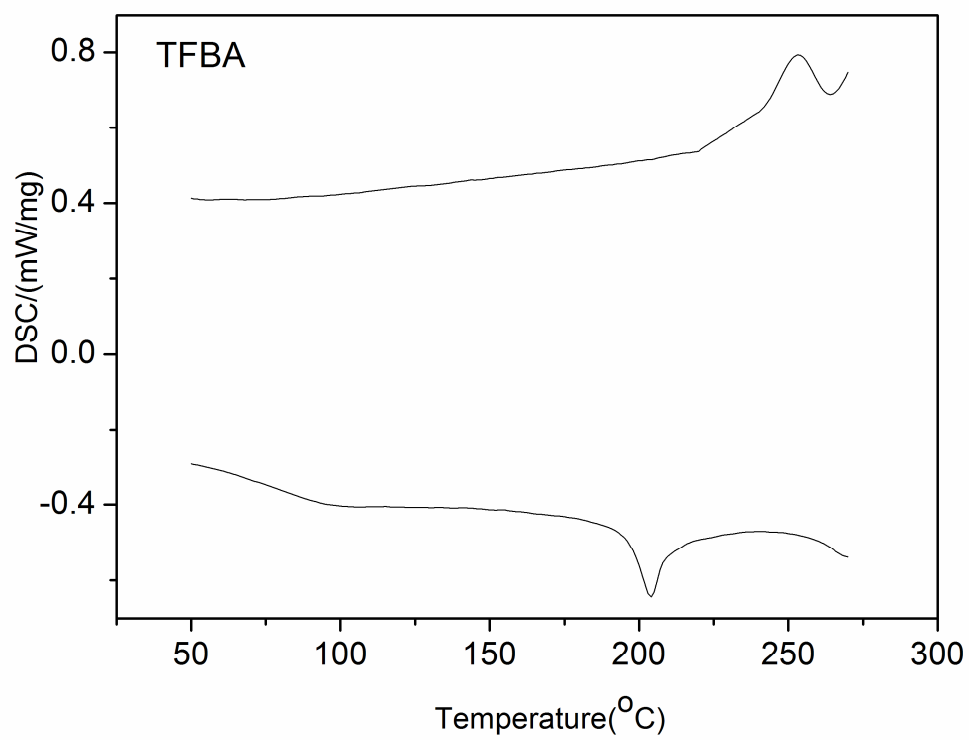
^cThe transition temperature obtained from POM.

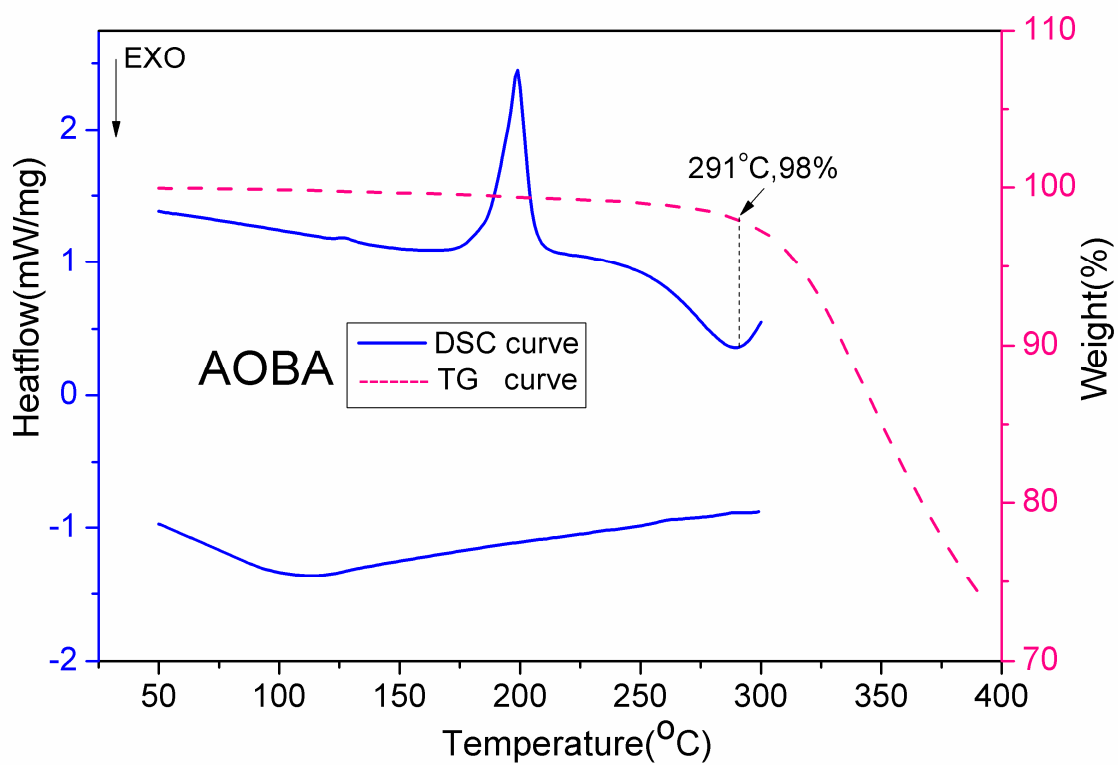


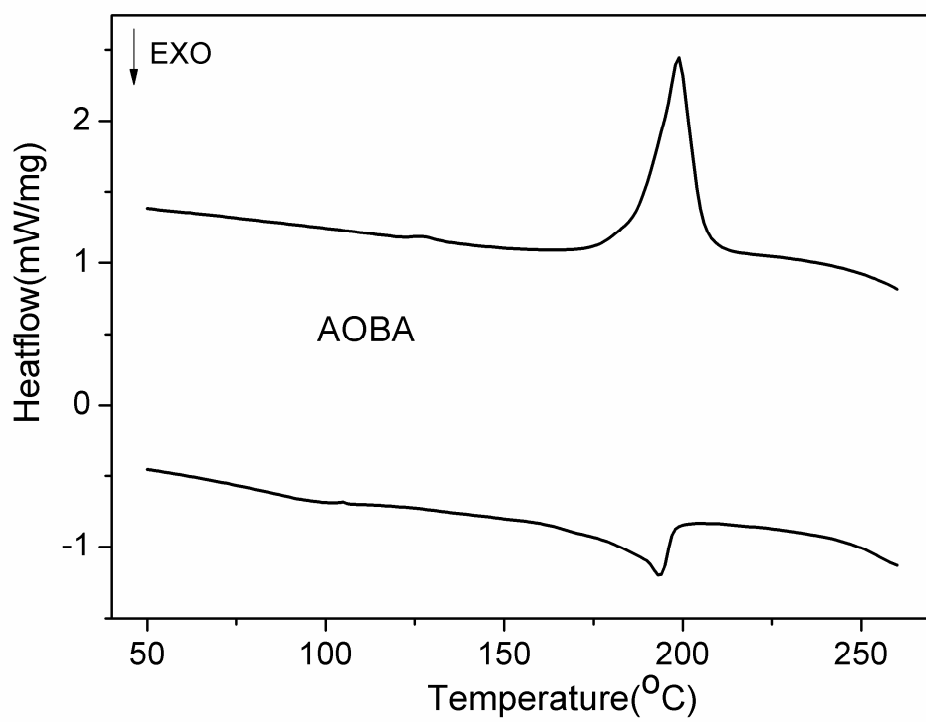


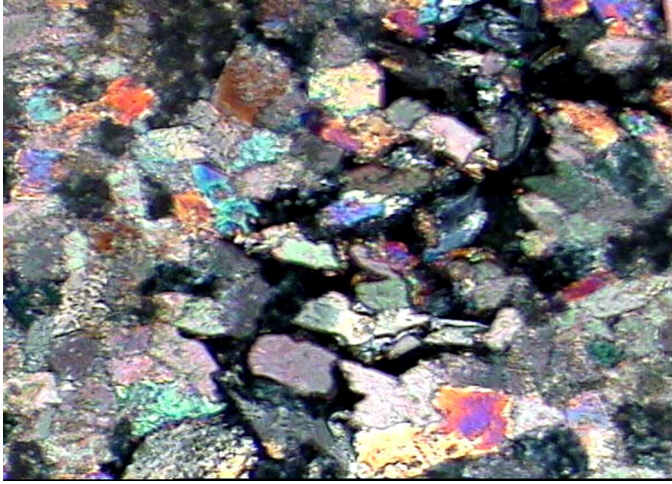
ACC



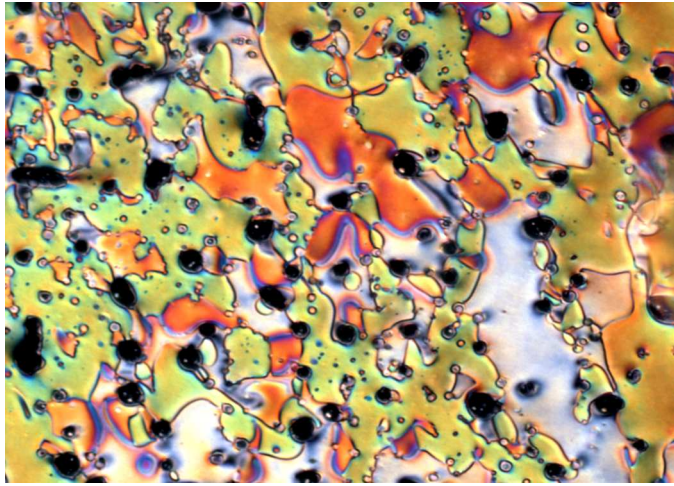




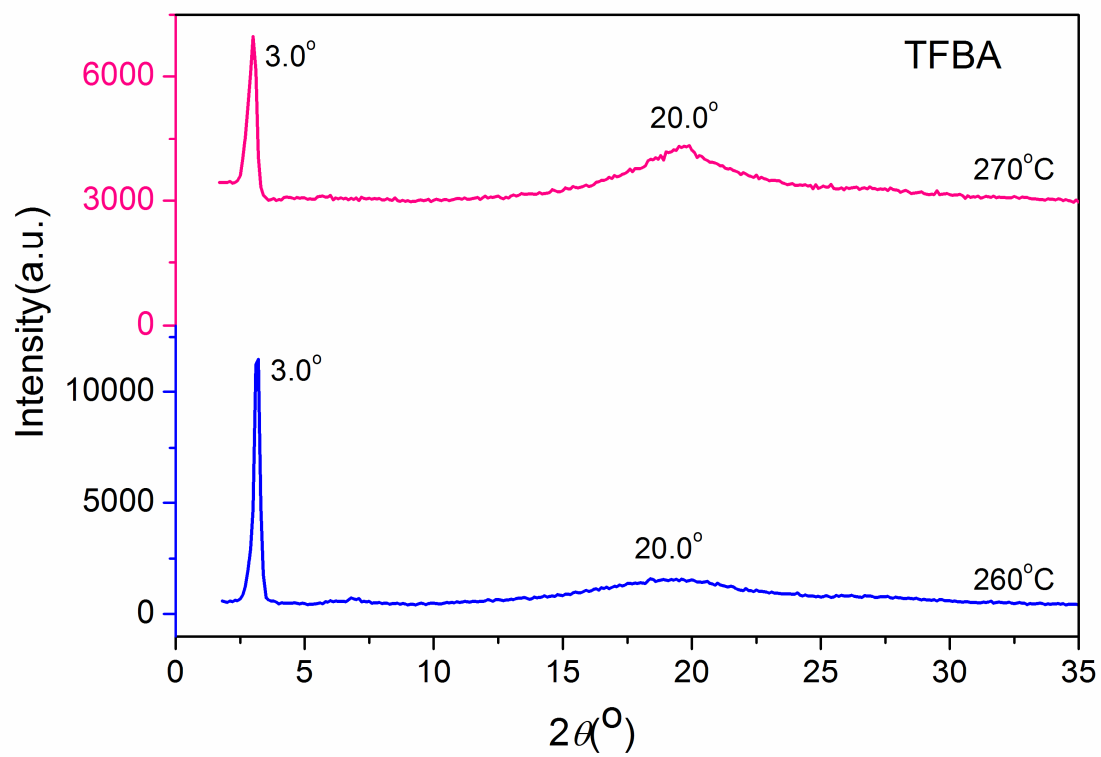


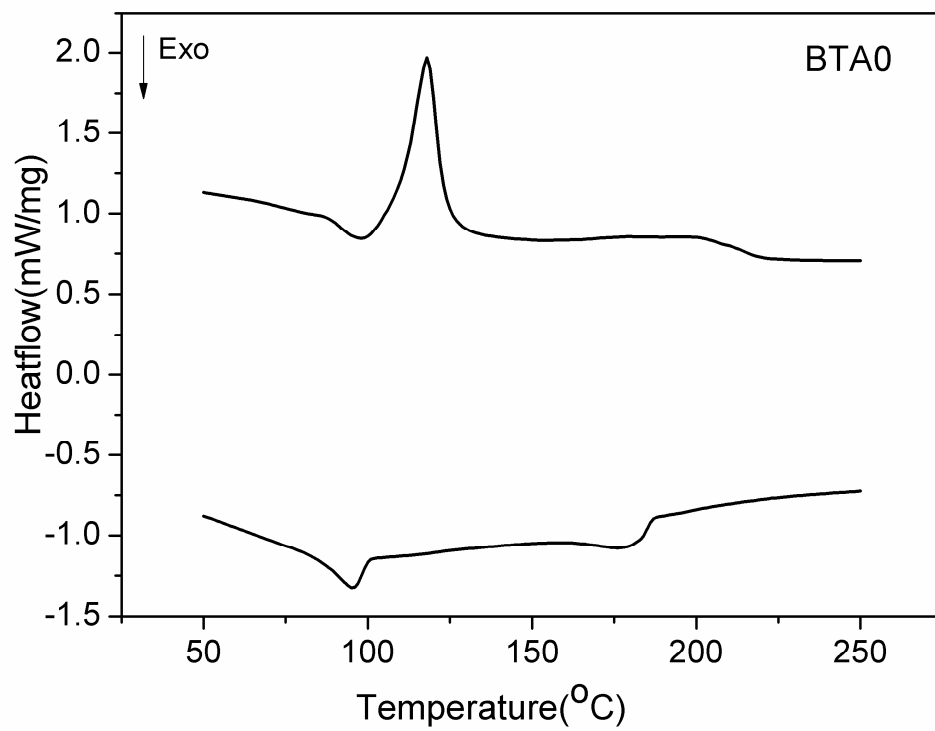


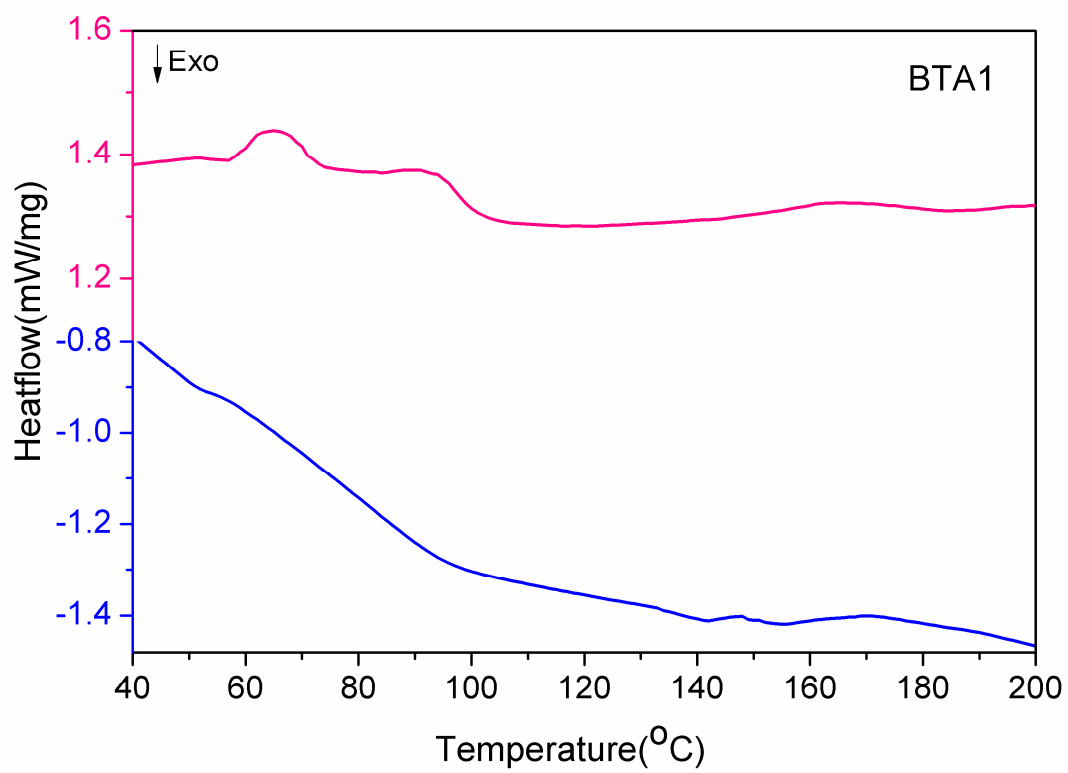
ACCEPTED MANUSCRIPT

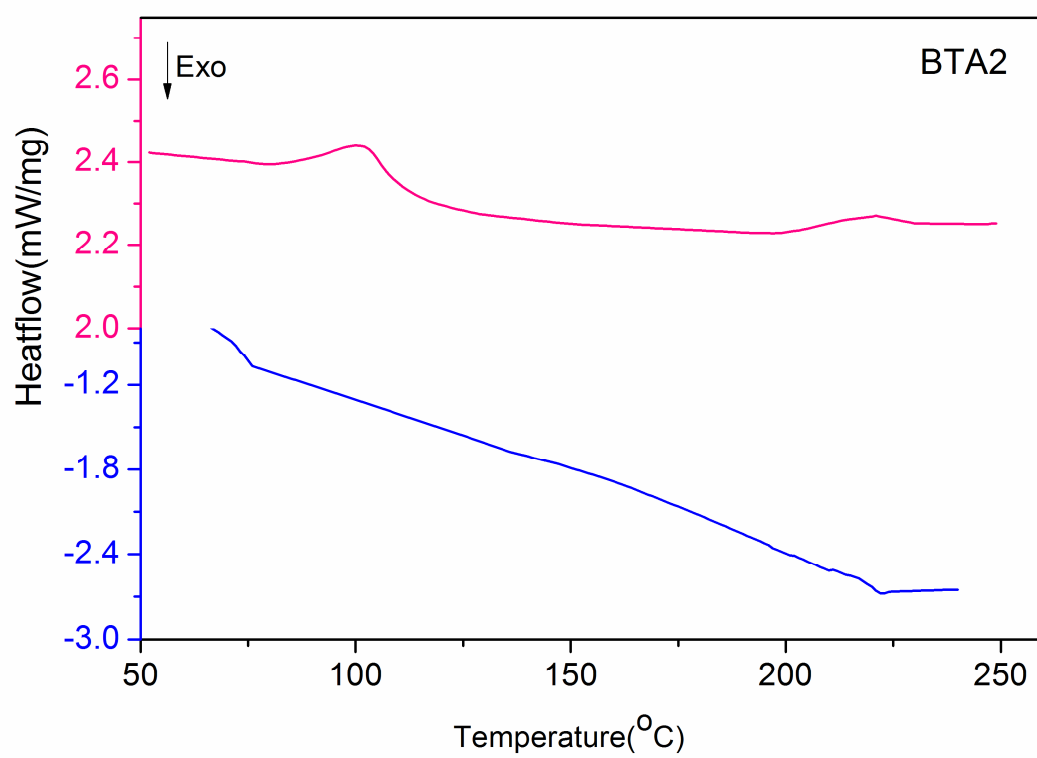


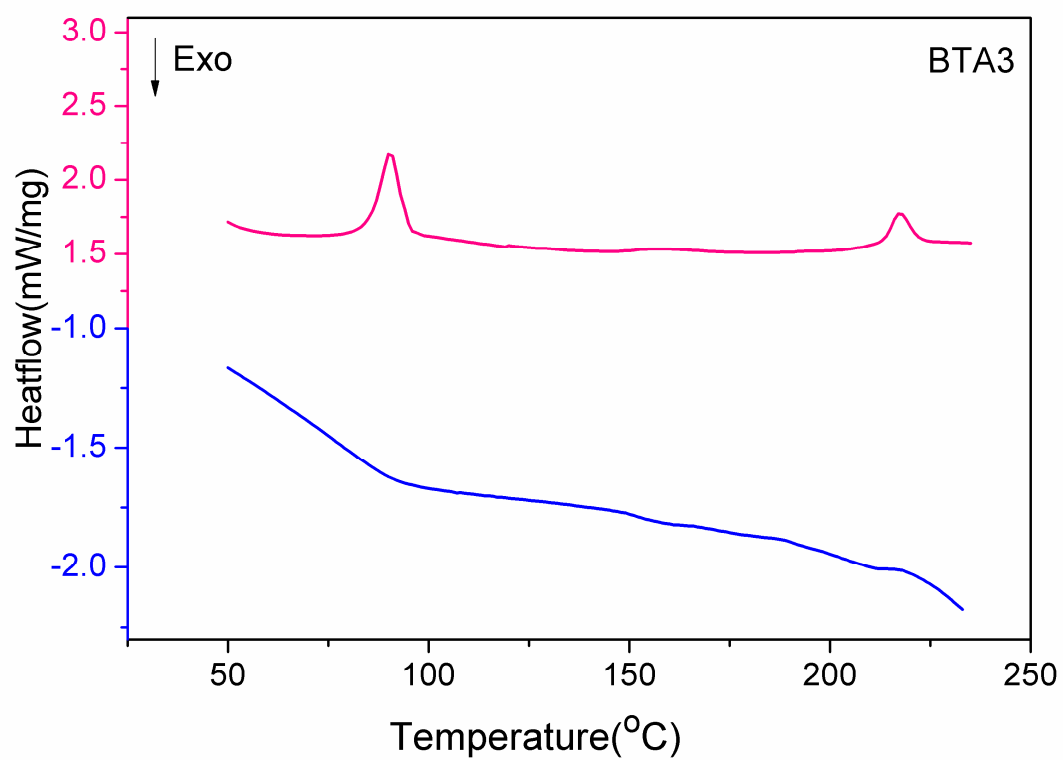
ACCEPTED MANUSCRIPT

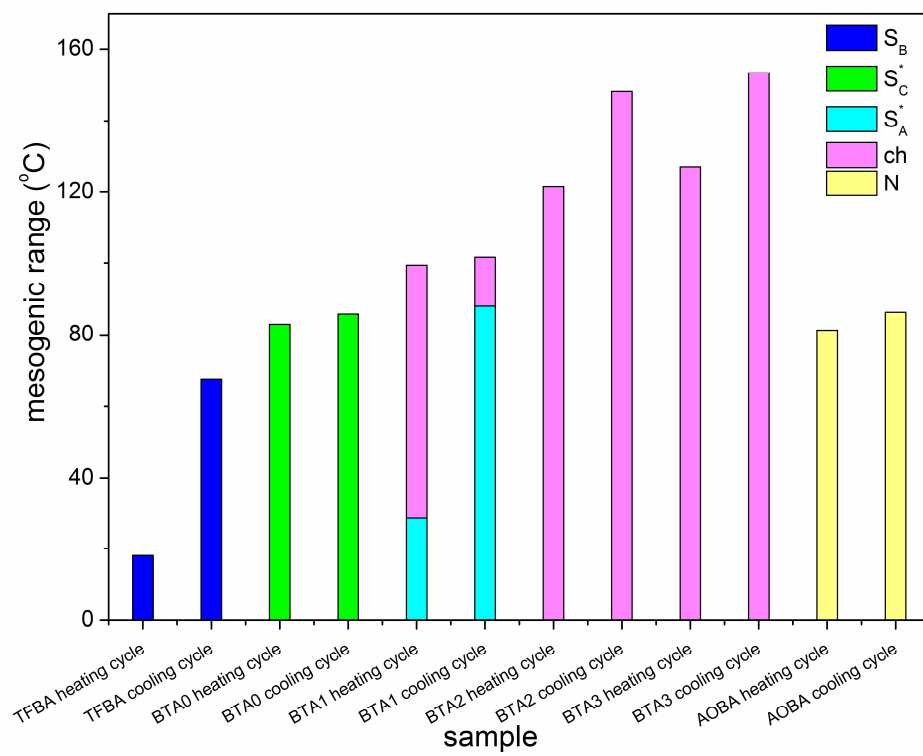


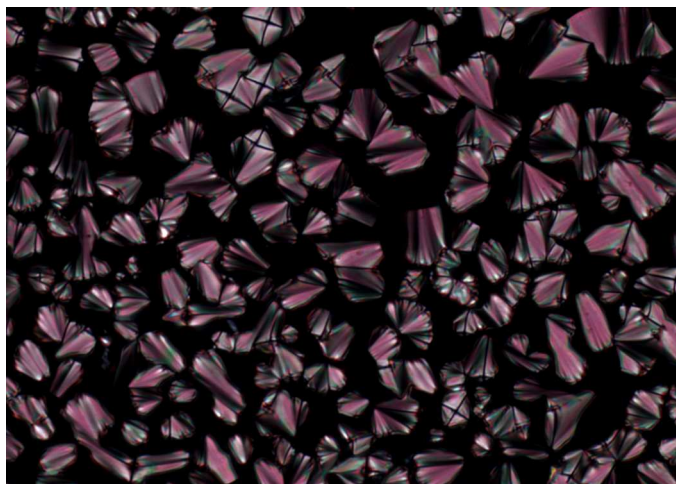




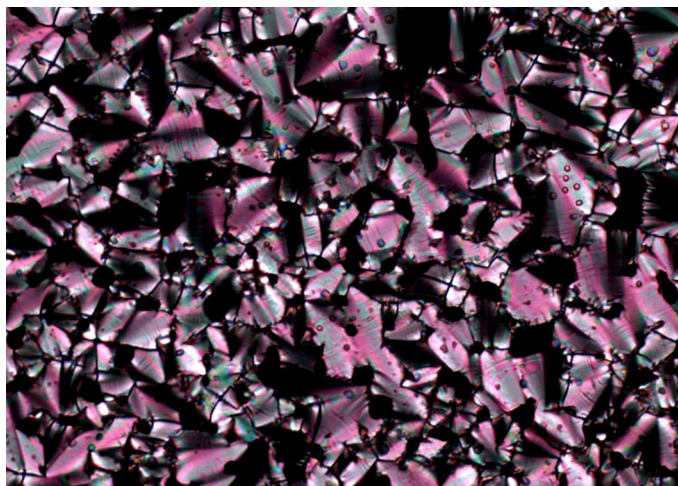




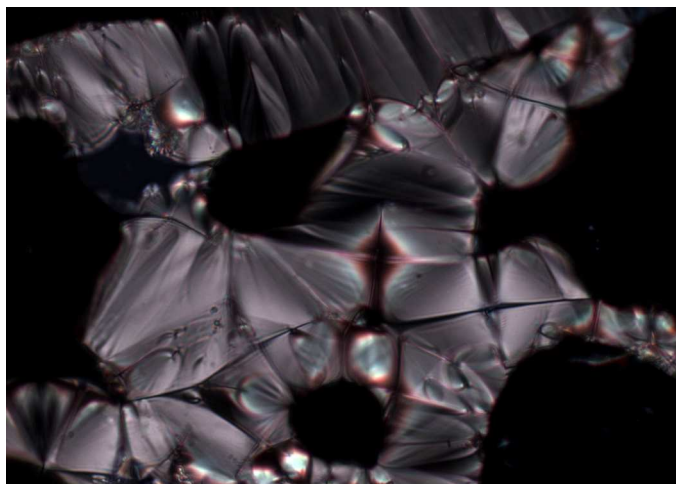




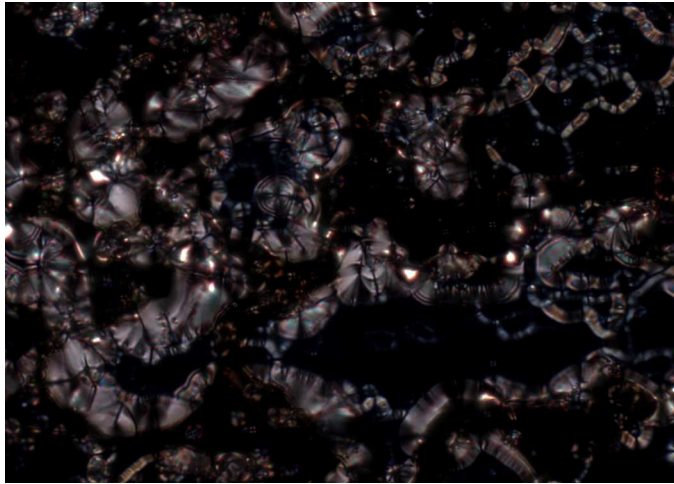
ACCEPTED MANUSCRIPT



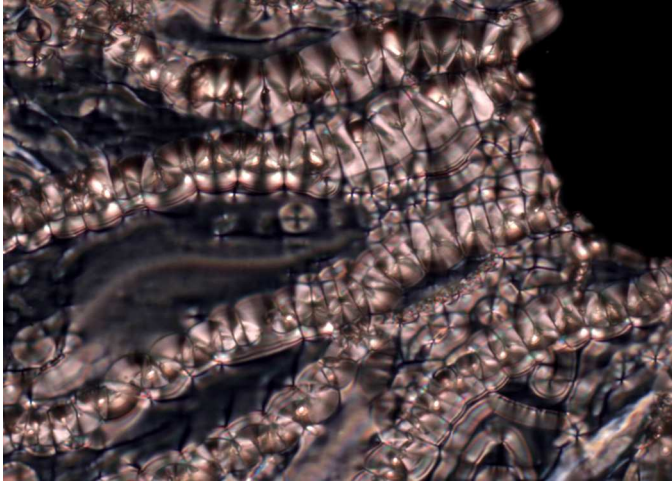
ACCEPTED MANUSCRIPT



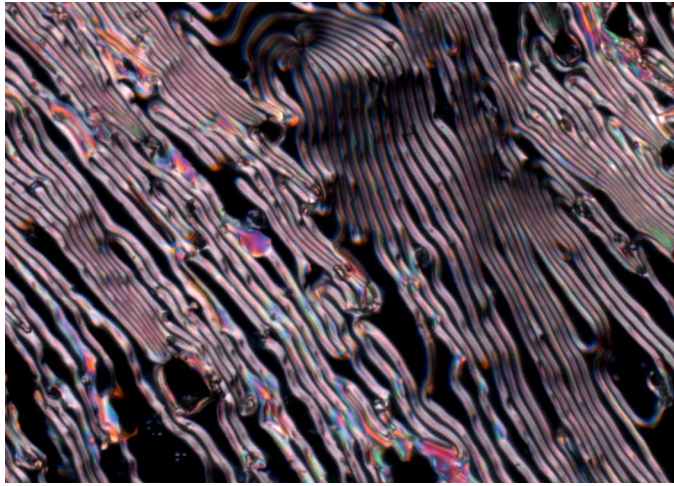
ACCEPTED MANUSCRIPT



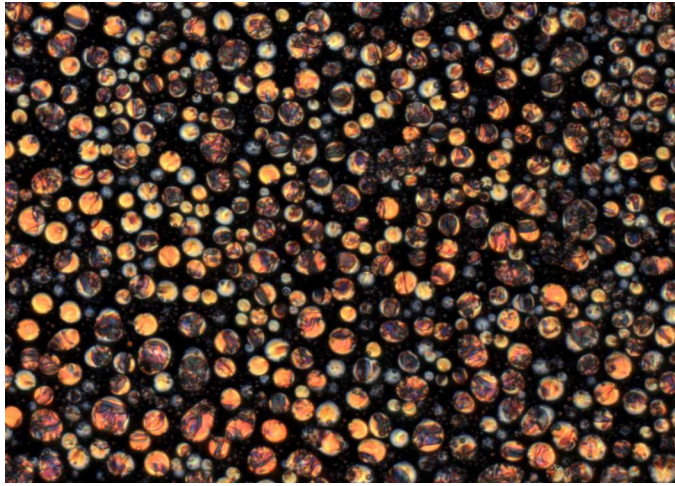
ACCEPTED MANUSCRIPT



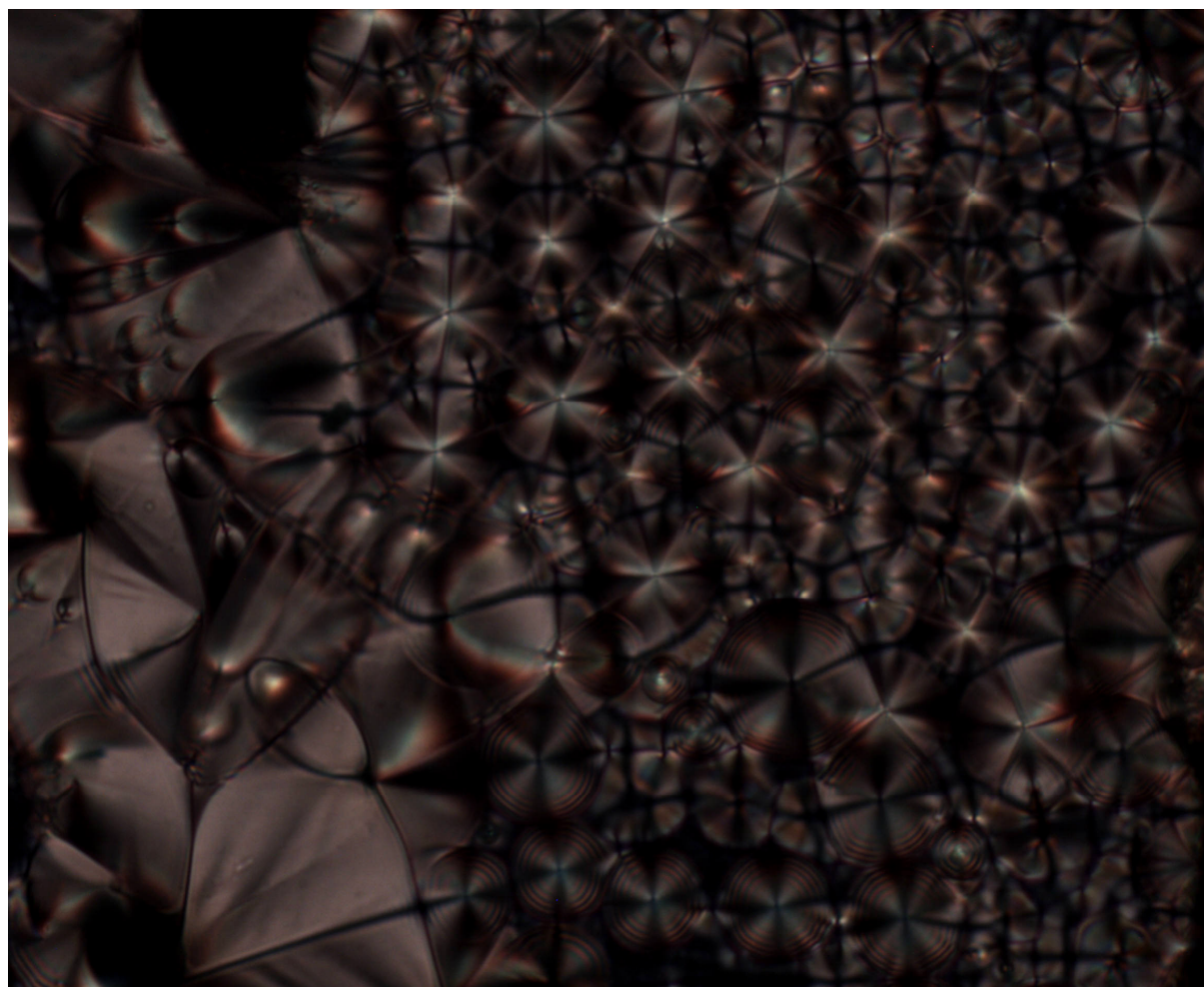
ACCEPTED MANUSCRIPT



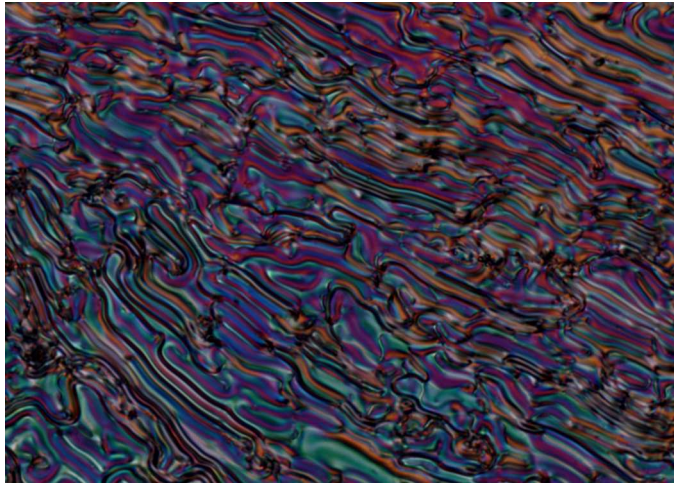
ACCEPTED MANUSCRIPT



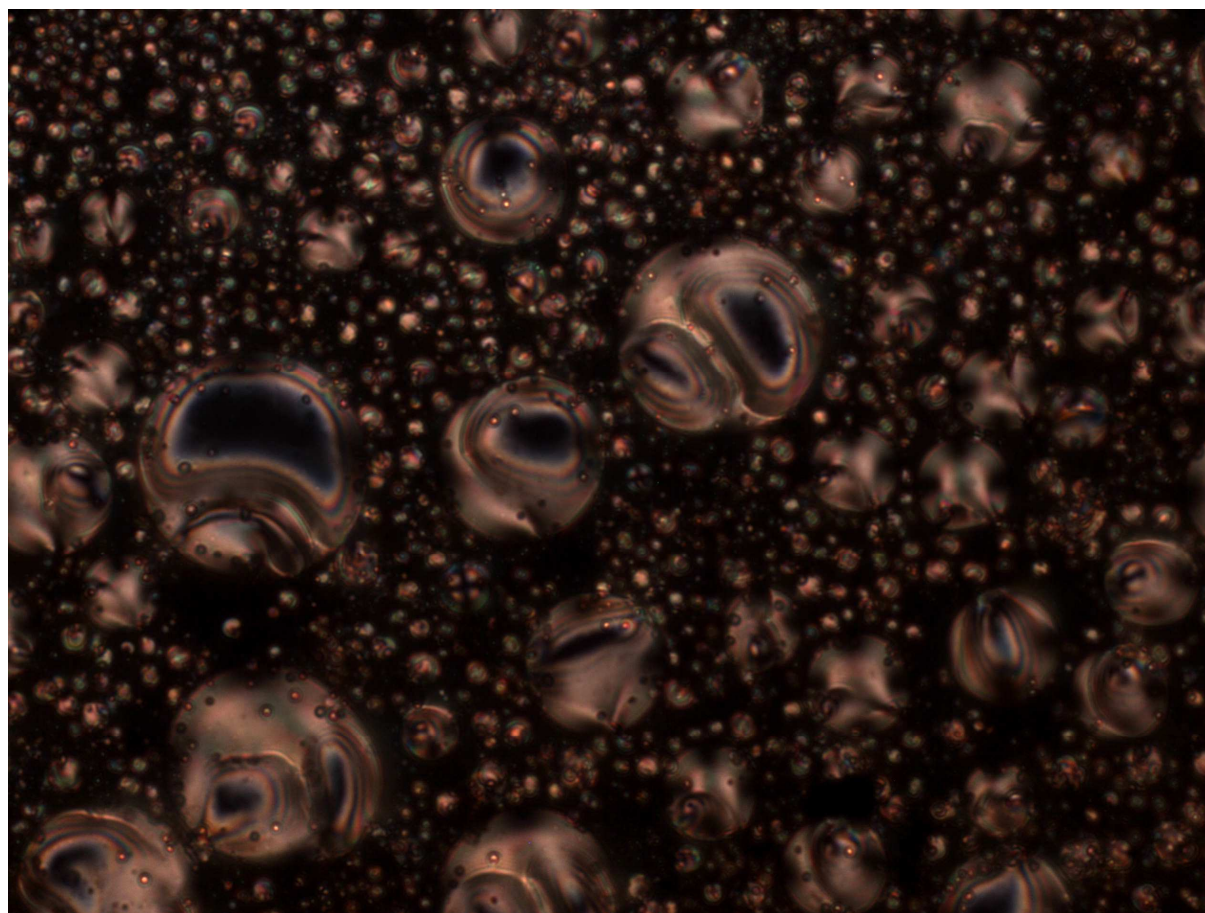
ACCEPTED MANUSCRIPT



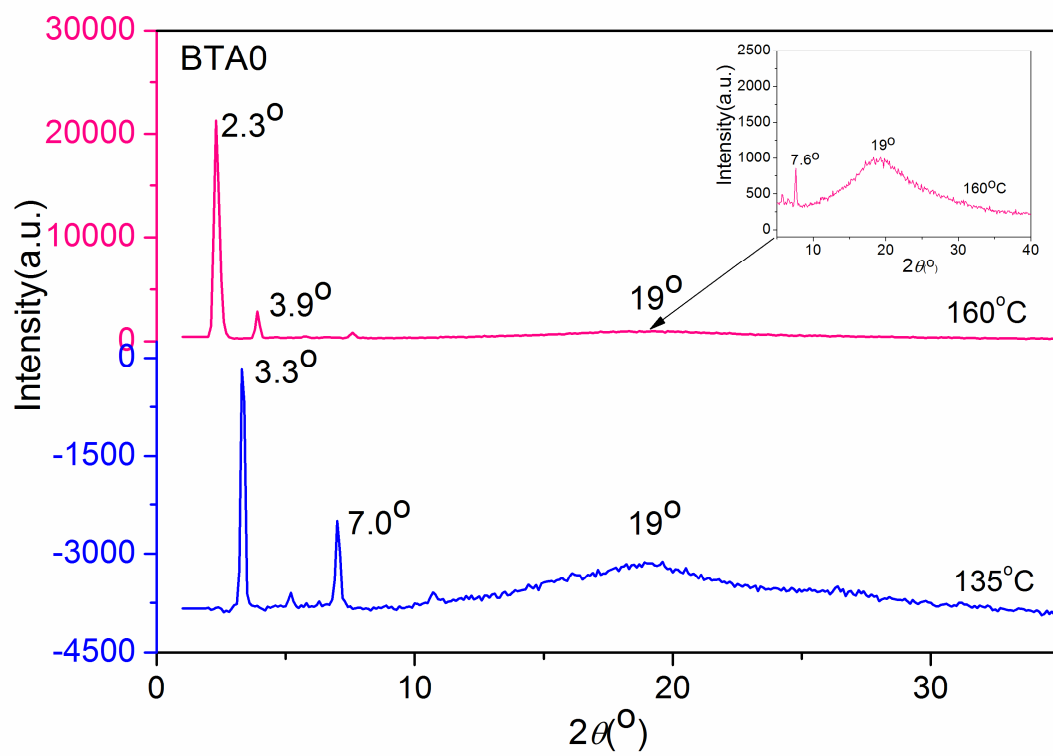
ACCEPTED

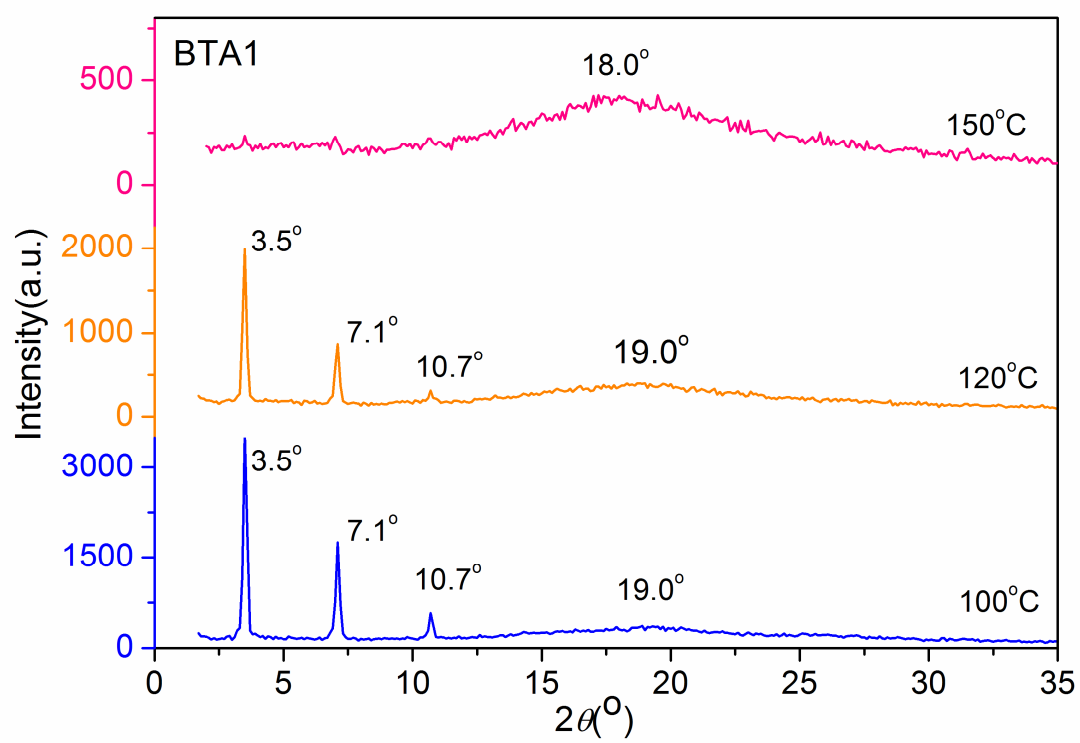


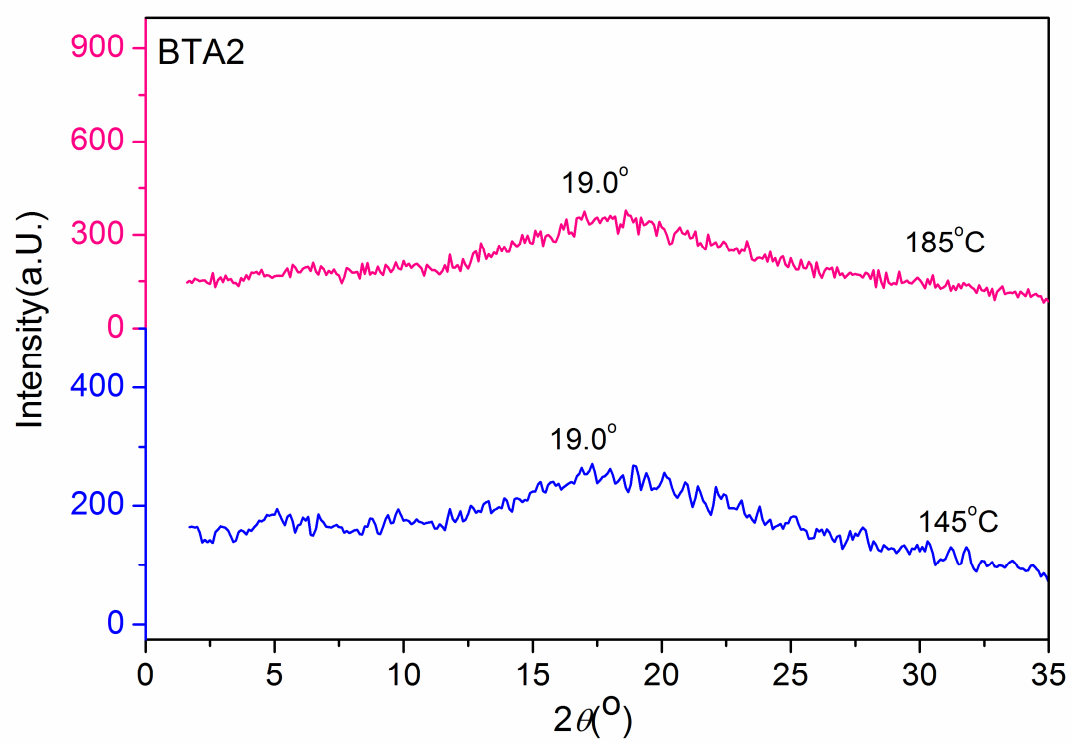
ACCEPTED MANUSCRIPT

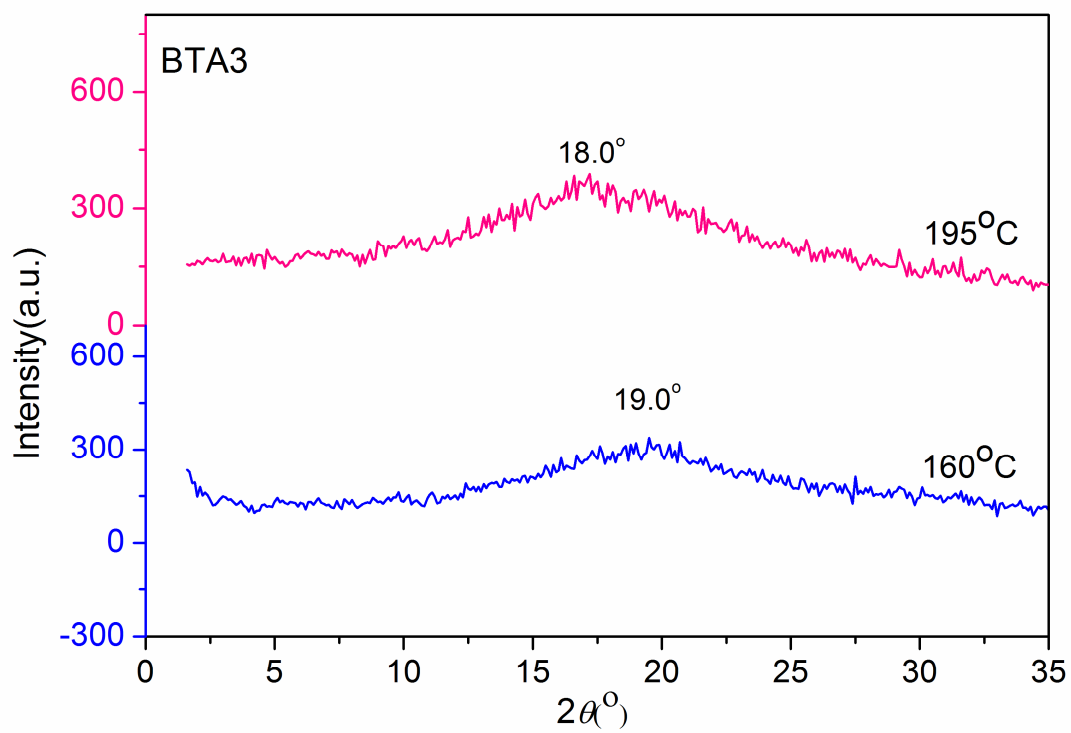


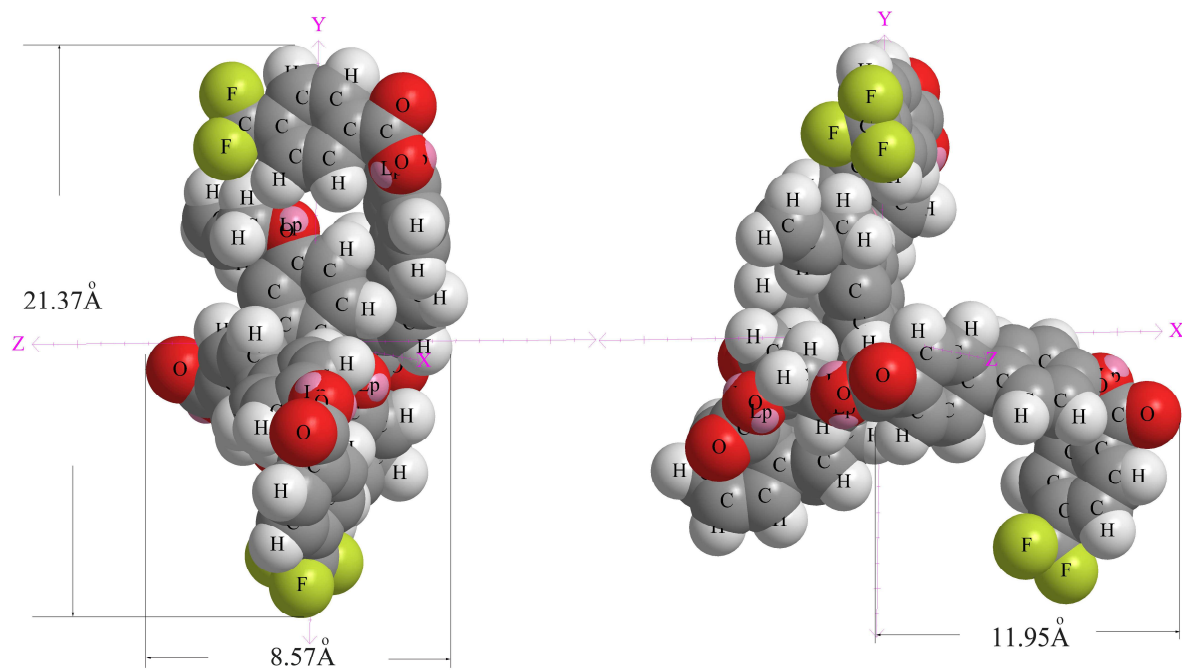
ACCEPTED MANUSCRIPT







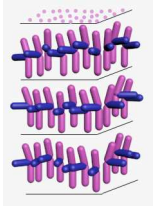




A. Front view

B. Left view

ACCEPTED MANUSCRIPT



ACCEPTED MANUSCRIPT

Highlights

Synthesis of symmetrical and asymmetrical three-arm liquid crystals with 1, 2, 4-butanetriol as chiral core.

The asymmetrical three-arm liquid crystals have both nematic and smectic liquid crystal side arms in them.

We have analyzed the three-arm liquid crystals using variable-temperature X-ray diffraction, DSC and POM.

The three-arm liquid crystal, whether symmetrical or asymmetrical, displayed cholesteric phase when the nematic liquid crystal side arm was introduced into it.

The smectic three-arm liquid crystals displayed layers of different thickness.